Road pavement macrotexture estimation at the design stage

Road pavement macrotexture estimation at the design stage

Filippo Giammaria Praticò[a] **and Rosario Fedele**[a]

[a] DIIES Department, University "Mediterranea" of Reggio Calabria, Via Graziella - Feo di Vito - 89100 Reggio Calabria – ITALY. Email: filippo.pratico@unirc.it

[a] DIIES Department, University "Mediterranea" of Reggio Calabria, Via Graziella - Feo di Vito - 89100 Reggio Calabria – ITALY. Email: rosario.fedele@unirc.it

Corresponding author: rosario.fedele@unirc.it

Abstract

Road performance (e.g., rolling resistance, friction, noise, and hydroplaning) is affected by surface macrotexture. The characteristics above need to be controlled and predicted at the design stage because of the consequences on sustainability and safety. However, macrotexture is quite difficult to govern when designing a mixture and this fact poses many issues, especially when focusing on Low-nominal maximum aggregate size, NMAS, mixtures. Consequently, tools are needed, at the design stage, to better predict a pavement surface macrotexture (e.g., mean texture depth, MTD). For these reasons, the main objective of this study is to set up and implement a model to predict MTD at the design stage. To this end, three main data sets of bituminous mixtures were taken into account. The first data set was created considering technical specifications limits, the second one consisted of data from the literature, and the third one consisted of mixtures especially created in the laboratory (low-NMAS mixtures). Modelling was carried out by setting up several equations, which are based on the sphere packing model and on the concept of filling volume, FV, herein introduced. Results demonstrate that (1) NMAS and FV can explain up to 88% of MTD variance, (2) the lower specification limits set up in technical specifications must not be considered as good descriptors of the expected MTD, and (3) for low-NMAS mixtures the impact of FV appears less important, while the impact of NMAS seems to be still important. Results can benefit both researchers and practitioners.

Key words: Low-noise; Low-NMAS; Air void content; Mean Texture Depth modelling; Filling volume; Road pavement; Specifications limits

1. Introduction

Road performance (e.g., rolling resistance, friction, noise, and hydroplaning) is affected by surface macrotexture (e.g., mean texture depth, MTD). The characteristics above need to be controlled and predicted at the design stage because of the consequences on sustainability and safety [1–3].

In more detail, **rolling resistance** is the force resisting the motion when a vehicle moves on a road. The rolling resistance coefficient, RRC, is the ratio between the rolling resistance and the normal force. RRC depends on speed usually with a negative correlation, i.e., RRC decreases when speeds increase. RRC depends also on air temperature (usually positive correlation), tyres, and surface texture (e.g., macrotexture and roughness, with positive correlations). RRC typically varies from 0.005 to 0.02. In the literature (cf. [4][5][6]), RRC is often supposed to depend linearly on mean profile depth, MPD (and sometimes also on IRI, cf. MIRIAM project report cited in [4]):

$$RRC \cong 0.0017 \cdot MPD + 0.0093 \tag{1}$$

The relationship above uses the mean profile depth, MPD, mm (ISO 13473-1), instead of the mean texture depth, MTD, mm (ISO 13473-1). Even if different relationships are given, especially for porous asphalts [7], based on ASTM E 1845 [8], it is:

$$MTD = 0.8 \cdot MPD + 0.2 \tag{2}$$

Figure 1.a illustrates how RRC (dimensionless) varies as a function of MTD (mm), where the pictogram ☹ points out that the given condition does not comply with main road engineering objectives (high rolling resistance and friction, and low water film thickness and noise level) and *vice versa*.

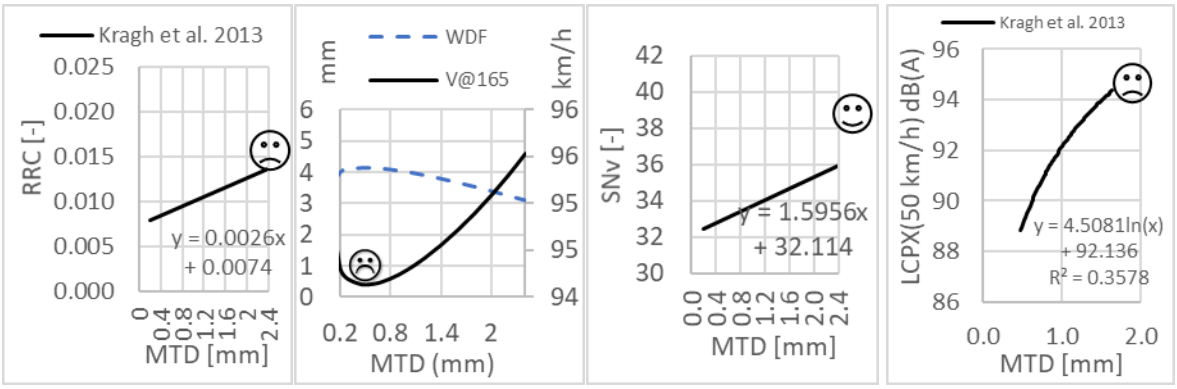

(a) (b) (c) (d)

Figure 1. MTD versus RRC, HPS, friction, and noise.

The hydroplaning speed, HPS (Fig. 1.b), refers to the speed that can lead to a complete loss of contact and friction between tyre and road. It depends on water film depth (WFD), on the length of wet track, on the presence of lubricants, on the tyre pressure (positive correlation), on tyre tread, on pavement capacity to drain away water, on pavement macrotexture, on type of contact, on road geometry, on pavement type (cf. PAVDRN model), on vehicle type (e.g., car or truck), and on the type of wheel system (all-wheel, front-wheel, rear-wheel drive, cf. [9–12]). It is noteworthy that the hydroplaning speed is an indirect measure of the effect of macrotexture on friction loss due to contact loss for a given scenario (including macrotexture level). For tyre pressures of about 2.0-2.5 bars, for cars, HPS is usually 60-100 km/h. HPS can be estimated using many models, including the Gallaway model [9–11]:

$$HPS = 0.9143 \cdot SD^{0.04} \cdot p_t^{0.3} \cdot (0.794 + TD)^{0.06} \cdot A, \quad (3)$$

where HPS is the hydroplaning speed (km/h), SD is the spindown of the tire rotational speed at the initiation of hydroplaning (%), p_t is the tyre pressure (kPa), TD is the tyre tread depth (mm), and A is a parameter that can be estimated using the following equation:

$$A = max\left(\frac{12.639}{WFD^{0.06}} + 3.50\,;\left[\frac{22.351}{WFD^{0.06}} - 4.97\right] \cdot TXD^{0.14}\right). \quad (4)$$

In Eq. 4, TXD=MTD is the mean texture depth (mm), while WFD stands for Water Film depth (mm). In turn, WFD can be estimated using the following expression:

$$WFT = 0.01485\left[\frac{TXD^{0.11}\cdot L^{0.43}\cdot I^{0.59}}{S^{0.42}}\right] - TXD, \tag{5}$$

where L is the drainage path length (m), I is the rainfall intensity (mm/h), and S is the pavement cross slope (m/m).

Figure 1.b illustrates how HPS (solid line, V@165) and WFD (dotted line) vary as a function of MTD (x-axis), under the following assumptions: MTD: varied, flow path length: 60 m, rainfall intensity: 80 mm/h, flow path slope: 3%; spin down speed: 10%, tyre pressure: 165 kPa, Tyre tread depth: 0.5 mm (cf. [9–12]).

The synergy between macro- and micro-texture in determining **pavement-tyre friction** is somehow far from being well assessed. Indeed, pavement-tyre friction encompasses many contributions, including: 1) Rubber adhesion force (to the pavement, especially in dry conditions); 2) Rubber hysteresis force (caused by tire deformation and related to rolling resistance). Especially in wet/wet and flooded conditions, 3) Rubber cohesion force (which is needed to break the interface contaminant bond); and 4) Air and fluid drag force ([16]).

Micro-texture can be assessed for example in terms of PTV (British pendulum, cf. [13–19]) or DFT (ASTM E 1911), while macrotexture can be assessed for example in terms of MTD.

In wet conditions, friction is affected by macrotexture mostly because of permeability and wet contact impact. At the same time, in dry conditions, friction could be affected by macrotexture because of dissipated energy (cf. [20]). To this end, it is noted that by referring to the attempt to conceptualise the transition from one friction measurement method to another one *via* the use of macrotexture parameters (International Friction Index, PIARC experiment [21], and ASTM E 1960-07 [22]) further studies are needed (cf. [23,24]). Based on [25,26], a wet-related equation is as follows:

$$SN_V = \frac{154}{V^{0.77}}\cdot\left[TD^{0.05} + \frac{4.71\cdot MTD^{0.09}}{(25.4\cdot WD + 2.5)^{0.09}}\right], \tag{6}$$

where SN_V is the skid number at a vehicle speed V (mph), TD stands for tire tread depth (in), and WD represents the water film thickness (in). Note that this model is applicable for passenger cars with tires with an inflation pressure of 165.5 kPa. Figure 1.d illustrates how MTD affects friction. Note that the parameter SN50 in Fig. 1.c was derived using Eq. 6, with V = 50 km/h, TD = 0.5 mm, and WD = 4 mm.

Traffic noise and particularly **rolling noise** are affected by macrotexture mainly because of MTD relationship with generation factors (Weyl-Van Der Poel's equation [27]), porosity, tortuosity, and resistivity (cf. [28,29]). Figure 1.d shows how MTD affects LCPX(50) (where LCPX(50) is the sound pressure level of the rolling noise measured using the Close Proximity, CPX, method at 50 km/h, based on [30]).

Finally, Fig. 2 illustrates how the four selected parameters above are affected by MTD, in terms of percentages. Note that curves were normalized with respect to MTD = 1 mm. Even if these values are partly biased due to the interaction between MTD (x-axis) and other factors (e.g., AV), Fig. 2 points out that high values of MTD (e.g., five times higher, from 1 mm to 5 mm) imply an increase of rolling resistance (solid line, +105%), noise (dashed line, +8%), friction (solid line with circular marker; +15%), and hydroplaning speed (dotted line, +8%). In contrast, when MTD decreases towards lower values (domain of low-NMAS mixtures), for values of MTD five times smaller (i.e., from 1mm to 0.2 mm, flat surface), rolling resistance (-21%), noise (-8%,), and friction (-23%) decrease, while the hydroplaning speed does not undergo tangible variations. It is worth noting that the potential decrease of macrotexture and friction for MTDs lower than 1mm, is even more critical when designing low-noise mixtures, because a balance must be pursued among concurring instances (e.g., acoustic impact and safety), based on a few parameters such as aggregate gradation, bitumen percentage, and compaction effort.

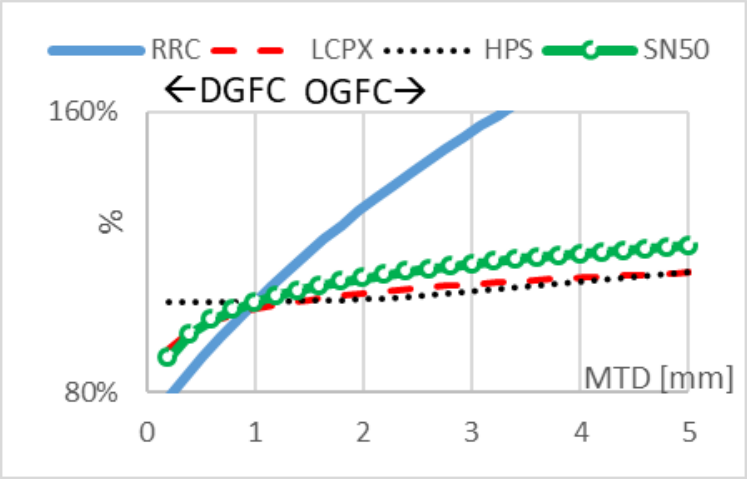

Figure 2. MTD versus parameters percentage.

Unfortunately, despite the impact of macrotexture on the quoted characteristics, macrotexture is quite difficult to govern when designing a mixture and this fact poses many issues especially when focusing on Low-Nominal Maximum Aggregate Size, NMAS, mixtures. Consequently, at the design stage, tools are needed to better predict a pavement surface macrotexture.

Based on the above, the main objective of the study presented in this paper is to set up and validate a model to use at the design stage for the estimation of pavement surface macrotexture (cf. Fig. 3).

In pursuing the objective above (cf. Fig. 3):

A. Three data sets were populated (bringing with their combinations to seven possible data sets):
    i. Requirements (data set RE). Indeed, these data are the main support during mix design.
    ii. Literature (data set LI). This set is crucial because entails the effect of processes.
    iii. Experiments (data set EX). This set is essential because refers to the specific issue.
B. A model was set up and implemented in terms of two main equations.
C. As a part of model finalization, eight expressions for the “filling volume” (concept and eight parameters herein introduced) were set up and implemented.
D. The level of compaction considered was the one that corresponds to the use of technical requirements, that is to say the one of as-built pavements.

Overall, the following tasks were carried out:

Task 1. Background: analysis of contractual requirements (data set requirements, RE) and analysis of the literature (data set literature, LI), see section 2.

Task 2. Modelling: Macrotexture modelling based on a sphere packing model and introducing the concept of "filling volume" (see section 3).

Task 3. Experiments: Create and test low-noise hot mix asphalt specimens, data set EX (cf. section 4).

Task 4. Model implementation (cf. section 5): Validate the proposed model (see section 5). Task 4.1: 2 equations, 6 Filled Volumes, FVi, 6 data sets. Task 4.2: Calibrations using the data set LI; Task 4.3: validation using the data sets EX and RE);

Task 5. Conclusions and recommendations (see section 6).

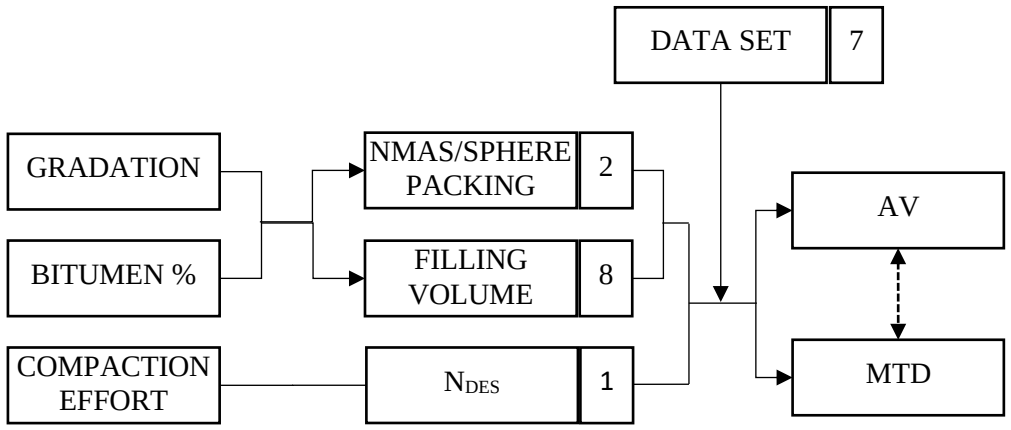

Notes: 1, 8, 2, 7= Number of cases considered.

Figure 3. Graphical abstract.

2. Background

This section illustrates how the data sets RE and LI were derived (task 1). Table 1 shows the requirements (RE) used in this study. In particular, based on two main Italian documents (i.e., CIRS and ANAS, respectively; cf. [31,32]), Dense Graded Friction Course (DGFCs), Open Graded Friction Course (OGFCs), Very Thin Layers, and "Splitmatix" mixtures were taken into account.

Tab. 1. Reference requirement (CIRS and ANAS documents).

Mix	**DGFCs**	
Ref.	CIRS [31]	ANAS [32]

Tentative name	CIRS-DGFC-A	CIRS-DGFC-B	CIRS-DGFC -C	CIRS-DGFC(m)-A	CIRS-DGFC(m)-B	CIRS-DGFC(m)-C	ANAS-DGFC-A	ANAS-DGFC-B	ANAS-DGFC(ms)-A	ANAS-DGFC(ms)-B	ANAS-DGFC(mh)-A	ANAS-DGFC(mh)-B	ANAS-DGFC-A+Foam Clay
Thickness [cm]	5.00	3.50	2.50	5.00	3.50	2.50	5.00	3.00	5.00	3.00	5.00	3.00	5.00
P_{sand}	23.5	23.5	28.5	23.5	23.5	28.5	23.5	27	23.5	27	23.5	27	23.5
Gse_{sand}	2.75	2.75	2.75	2.75	2.75	2.75	2.75	2.75	2.75	2.75	2.75	2.75	2.75
P_{filler}	8.00	8.00	8.00	8.00	8.00	8.00	8.00	8.00	8.00	8.00	8.00	8.00	8.00
Gse_{filler}	2.93	2.93	2.93	2.93	2.93	2.93	2.93	2.93	2.93	2.93	2.93	2.93	2.93
$P_{4.75}$	47.5	50	55	47.5	50	55	49	54	49	54	49	54	49
$Gse_{4.75}$	2.75	2.75	2.75	2.75	2.75	2.75	2.75	2.75	2.75	2.75	2.75	2.75	2.75
$Gse_{4.75app}$	2.76	2.76	2.76	2.76	2.76	2.76	2.76	2.76	2.76	2.76	2.76	2.76	2.76
Pb	5.3	5.5	5.7	5.3	5.5	5.7	5.3	5.3	5.3	5.3	5.3	5.3	6.1
Gb	1.02	1.02	1.02	1.02	1.02	1.02	1.02	1.02	1.02	1.02	1.02	1.02	1.02
AVdes	5	5	5	5	5	5	4.5	4.5	4.5	4.5	4.5	4.5	4.5
Ndes	100	100	100	100	100	100	120	120	130	130	140	140	120
D	150	150	150	150	150	150	100	100	100	100	100	100	100
NMAS	10.0	10.0	8.9	10.0	10.0	8.9	12.5	8.0	12.5	8.0	12.5	8.0	12.5
ΔMTD	0.2	0.2	0.2	0.2	0.2	0.2	0.2	0.2	0.2	0.2	0.2	0.2	0.2
MTDmin	0.4	0.4	0.4	0.4	0.4	0.4	0.4	0.4	0.4	0.4	0.4	0.4	0.4

Mix	**OGFCs**			**M**			**S**		
Ref.	CIRS [31]	ANAS [32]	ANAS [32]	CIRS [31]	ANAS [32]	ANAS [32]	CIRS [31]	CIRS [31]	CIRS [31]
Tentative name	CIRS-OGFC	ANAS-OGFC	ANAS-OGFC + Foam Clay	CIRS-M	ANAS-M-HOT	ANAS-M-COLD	CIRS-S 0/12	CIRS-S 0/8	CIRS-S 0/5
Thickness [cm]	4.5	5	4	0.7	0.65	0.65	0.8	0.6	0.3
P_{sand}	9	3	3	12.5	40.5	35	15	13	11
Gse_{sand}	2.75	2.75	2.75	2.75	2.75	2.75	2.75	2.75	2.75
P_{filler}	6.00	6.00	6.00	7.50	7.50	7.50	10.00	10.00	10.00
Gse_{filler}	2.93	2.93	2.93	2.93	2.93	2.93	2.93	2.93	2.93
$P_{4.75}$	20	12.5	11	25	80	65	42.5	39	95
$Gse_{4.75}$	2.75	2.75	2.75	2.75	2.75	2.75	2.75	2.75	2.75
$Gse_{4.75app}$	2.76	2.76	2.76	2.76	2.76	2.76	2.76	2.76	2.76
Pb	5.5	5.3	5.8	5.5	5.3	7.5	7	7	7.5
Gb	1.02	1.02	1.02	1.02	1.02	1.02	1.02	1.02	1.02
AVdes	17	22	22	12	4.5	N/A	3	3	3
Ndes	50	50	50	50	100	N/A	50	50	50
D	150	100	100	150	100	N/A	150	150	150
NMAS	15.0	14.0	11.0	10.0	4.0	7.0	12.5	9.5	4.75
ΔMTD	0.2	0.2	0.2	0.2	0.2	0.2	0.2	0.2	0.2

MTDmin	0.8	1	0.8	0.6	0.5	0.3	0.5	0.5	0.5

Symbols [31][33]. DGFC and OGFC= Hot Mix Asphalt (HMA) Dense and Open Graded Friction Courses, respectively; A and B=Two reference gradation curves; m= HMA containing modified bitumen; M=Very Thin Layer consisting of HMA; S="Splitmatix" HMA mixture; P_{sand}=Percentage of sand in the mixtures (i.e., the difference between the passing percentage at the 2 mm sieve and the passing percentage at the 0.063 mm sieve; [dim.less] %); $P_{4.75}$=Passing at the 4.75 mm sieve [dim.less] (%); Gse_{sand}=Effective specific gravity of the sand [dim.less]; Gse_{filler}=Effective specific gravity of the filler [dim.less]; $Gse_{4.75}$=Effective specific gravity of the $P_{4.75}$ [dim.less]; $Gse_{4.75app}$=Approximated Effective specific gravity of the $P_{4.75}$, i.e. which include the passing percentage at the 0.063 mm sieve [dim.less]; Pb=Percentage of bitumen by weight of the mixture [dim.less] (%); Gb=Specific gravity of the bitumen [kg/m^3]; AVdes=As design air voids in the mixture; Ndes=As design number of gyrations of the superpave gyratory compactor to obtain specimens with air voids equal to AVdes [dim.less]; D=Specimen diameter [mm]; NMAS=a.k.a. MNS, is the largest sieve that retains some of the aggregate particles but generally not more that 10% by weight [mm]; MTD=Mean Texture Depth [mm]; ΔMTD=Tentative value to express the variance of MTD; MTDmin=lower limit of the MTD; N/A=Not Available.

Figure 4 and table 2 illustrate the aggregate gradation and main characteristics of the seventy-three mixtures used to populate the data set LI.

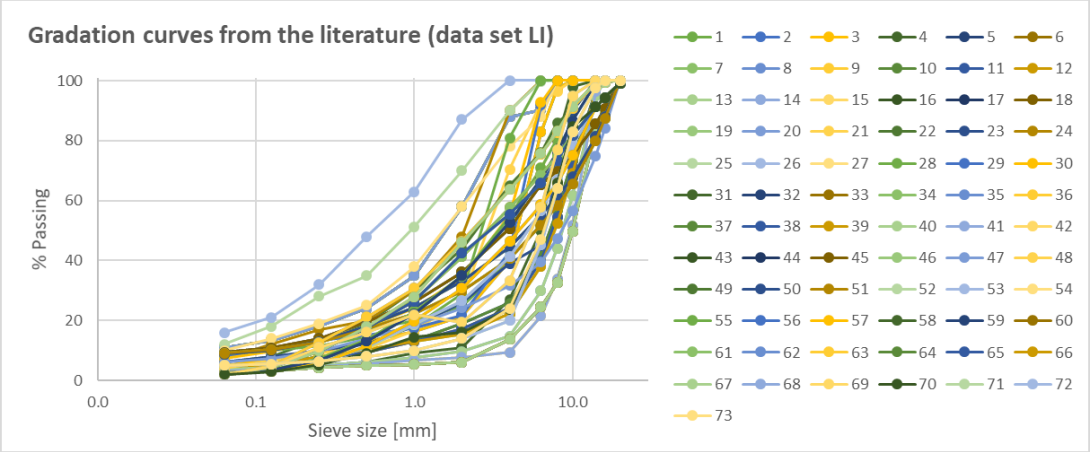

(a)

Mix	% Passing													Mix	% Passing												
#	20.0	16.0	14.0	10.0	8.0	6.3	4.0	2.0	1.0	0.50	0.25	0.125	0.063	#	20.0	16.0	14.0	10.0	8.0	6.3	4.0	2.0	1.0	0.50	0.25	0.125	0.063
1	100	100	100	100	98	83	40	25	20	17	13	11	9	38	100	90	85	50	33	24	14	6	5	5	4	3	3
2	100	100	100	100	98	83	40	22	16	13	10	7	5	39	100	90	85	50	33	24	14	6	5	5	4	3	3
3	100	100	100	100	98	83	40	22	16	13	10	7	5	40	100	90	85	50	33	24	14	6	5	5	4	3	3
4	100	100	100	98	80	50	27	11	9	6	5	4	2	41	100	91	86	75	70	65	51	36	26	20	14	11	9
5	100	100	96	73	57	42	26	19	13	10	8	5	4	42	100	91	86	75	70	65	51	36	26	20	14	11	9
6	100	100	96	71	55	40	24	17	13	9	7	5	4	43	100	87	80	66	58	52	41	30	22	17	13	10	9
7	100	100	96	69	52	38	22	15	13	10	8	5	4	44	100	91	86	75	70	65	51	36	26	20	14	11	9
8	100	100	95	62	44	30	15	10	7	6	5	4	4	45	100	91	86	75	70	65	51	36	26	20	14	11	9
9	100	100	96	52	34	21	9	8	7	6	5	4	3	46	100	87	80	66	58	52	41	30	22	17	13	10	9
10	100	100	96	73	57	42	26	19	13	10	8	5	4	47	100	84	75	57	47	39	32	24	18	14	10	7	6
11	100	100	96	71	55	40	24	17	13	9	7	5	4	48	100	88	81	68	61	55	44	33	24	18	13	10	9
12	100	100	96	69	52	38	22	15	13	10	8	5	4	49	100	88	81	68	61	55	44	33	24	18	13	10	9
13	100	100	95	62	44	30	15	10	7	6	5	4	4	50	100	88	81	68	61	55	44	33	24	18	13	10	9
14	100	100	96	52	34	21	9	8	7	6	5	4	3	51	100	87	80	66	58	52	41	30	22	17	13	10	9
15	100	100	100	100	100	90	88	58	35	24	18	13	11	52	99	94	91	79	67	56	41	27	19	11	6	4	2
16	100	100	100	100	100	90	88	58	35	24	18	13	11	53	99	94	91	79	67	56	41	27	19	11	6	3	2
17	100	100	100	100	100	90	88	58	35	24	18	13	11	54	100	100	99	91	81	71	55	35	23	14	7	3	2
18	100	100	100	100	100	90	88	58	35	24	18	13	11	55	100	100	99	91	81	71	55	35	23	14	7	3	2
19	100	100	100	100	100	90	88	58	35	24	18	13	11	56	99	94	91	75	66	59	47	31	20	11	6	3	2
20	100	100	100	100	100	90	88	58	35	24	18	13	11	57	99	94	91	75	66	59	47	31	20	11	6	3	2
21	100	100	100	100	97	93	70	27	17	11	9	7	4	58	100	100	99	87	76	67	53	35	22	13	7	3	2
22	100	100	100	90	86	76	65	44	30	19	14	8	6	59	100	100	99	87	76	67	53	35	22	13	7	3	2
23	100	100	100	90	70	45	39	26	18	12	10	8	6	60	99	94	91	82	75	69	58	41	27	18	10	4	2
24	100	100	100	100	100	100	90	48	30	20	17	12	7	61	99	94	91	82	75	69	58	41	27	18	10	4	2
25	100	100	100	100	100	100	90	70	51	35	28	18	12	62	100	100	99	91	83	76	64	46	31	21	13	5	2
26	100	100	100	100	100	100	100	87	63	48	32	21	16	63	100	100	99	91	83	76	64	46	31	21	13	5	2
27	100	100	100	100	100	88	78	58	38	25	19	14	10	64	99	94	91	82	73	66	55	42	26	18	10	4	2
28	100	100	100	100	100	100	81	29	18	15	12	10	9	65	99	94	91	82	73	66	55	42	26	18	10	4	2
29	100	100	100	100	100	92	43	22	17	15	13	11	8	66	100	100	99	91	83	76	64	46	28	18	10	4	2
30	100	100	100	100	100	93	55	34	24	18	14	10	7	67	100	100	99	91	83	76	64	46	28	18	10	4	2
31	100	90	85	50	33	24	14	6	5	5	4	3	3	68	100	100	100	95	77	58	33	19	22	16	11	5	2
32	100	90	85	50	33	24	14	6	5	5	4	3	3	69	100	100	100	95	77	58	33	19	22	16	11	5	2
33	100	90	85	50	33	24	14	6	5	5	4	3	3	70	99	94	91	85	66	46	24	16	15	9	5	3	2
34	100	90	85	50	33	24	14	6	5	5	4	3	3	71	100	100	98	83	64	45	20	14	10	8	6	5	5
35	100	90	85	50	33	24	14	6	5	5	4	3	3	72	100	100	98	83	64	45	20	14	10	8	6	5	5
36	100	90	85	50	33	24	14	6	5	5	4	3	3	73	100	100	98	83	64	47	24	14	10	8	6	5	5
37	100	90	85	50	33	24	14	6	5	5	4	3	3														

(b)

Figure 4. Aggregate gradations (data set LI): a) Gradation curves; b) Percentage passing.

Tab. 2. Reference asphalt concrete mixtures from the literature (data set LI).

	***NMAS* [mm]**		
***AV* (%)**	**10-18**	**7-10**	**0-7**
0-8	SMA16, SMA17, SMA18, CG14, CL14, CL11, FG13, FL13, PAC13	SMA8, SMA8+CR, AC10, SMA10, CG10, FG10, FL10, SMA9	ISO, AC5+CRD, AC6+CRW, WMA AC6+CRD
8-16	PAC16	SMA8+CR	AC6, AC6+CR
16-27	DL1, DL2 (PAC13+PAC20), PAC16, PAC12	PAC9	AC6+CR, PA6, AC4

Symbols. *NMAS*=Nominal Maximum Aggregate Size; *AV*=Air void content of the mixture; *SMA*=Stone Mastic Asphalt; AC=Asphalt Concrete; PAC=Porous Asphalt Concrete; DL=Double layer PAC; CG=Coarse Gravel; CL=Coarse Limestone; FG=Fine Gravel; FL=Fine Limestone; ISO=reference surface from ISO 10844; CRD=Crumb rubber added applying the Dry method; CRW=Crumb rubber added applying the Wet method; WMA=Warm Mix Asphalt. Note that: 1) all the mixtures, except for the WMA one are Hot Mix Asphalts. 2) The numbers after the acronym of the mixture are the Maximum Aggregate Sizes (*MAS*) or the *NMAS*.

References. SMA8, SMA8+CRW [14]; PAC9 [15]; DL1=(PAC13+AC20), DL2=(PAC13+PAC20)[34]; AC6, AC6+CRD, PAC6, AC10, SMA10, AC4 [35]; ISO=Reference surface of the ISO 10844 [36]; AC5+CRD, AC6+CRW, WMA AC6+CRD [37]; PA16 [38]; SMA16, SMA17, SMA18 [39]; CG14, CL14, FG13, FL13, FL10, SMA9, PAC13 [40]; PAC12 [41].

3. Modelling

The hexagonal packing model was used as a reference model to start to build the proposed model (Task 2). Note that this reference model allows obtaining a theoretical density (i.e., ratio between the volume of the spheres and the volume of the cube) of about 74 % [42]. Table 3 shows the logical framework that was followed to define the proposed model. Note that Eq. 8 was derived based on the definition of the average depth of pavement surface macrotexture (cf., EN 13036-1 [43]), the MTD can be considered as the ratio between *"a known volume of material on the surface and subsequent measurement of the total area covered".*

Tab. 3. Modelling.

Parameter	**Unit of measure**	**Equation**	**Equation number**
Side of a reference cube containing spheres of radius *r*	mm	$l = \frac{4 \cdot r}{\sqrt{2}}$	(7)
Area of the face of the cube	mm^2	$A_q = l^2$	(8)
Volume of the cube	mm^3	$V_c = l^3 = A_q \cdot \frac{r}{\sqrt{2}}$	(9)
Volume of the spheres inside the cube	mm^3	$V_s = 4 \cdot \frac{4}{3} \cdot \pi \cdot r^3$	(10)
Volume of voids into the cube containing the spheres	mm^3	$V_v = V_c - V_s$	(11)
Volume of bitumen into the asphalt concrete mixture	mm^3	$V_b = \frac{W_b}{\rho_b} = \frac{W_{mix} \cdot P_b}{\rho_b} =$ $= \frac{\rho_{mix} \cdot V_c \cdot P_b}{\rho_b} = l^3 \frac{\rho_{mix}}{\rho_b} \cdot P_b$ where W_b is the mass of the bitumen (g), ρ_b is the density of the bitumen (e.g., 0.00103 g/mm^3), and ρ_{mix} is the density of the mixture (e.g., 0.00234 g/mm^3).	(12)
Air void content	dim.less (%)	$AV = \frac{V_c - V_s - V_b}{V_c}$	(13)
Mean Texture Depth	mm	$MTD = \frac{V_c - V_s - V_b}{A_q} = \frac{V_c \cdot AV}{A_q} = \frac{l^3 \cdot AV}{l^2} =$ $= l \cdot AV = \frac{4}{\sqrt{2}} \cdot r \cdot AV = k \cdot r \cdot AV$ where k is a coefficient to calibrate.	(14)

3.1 Model generalization

Taking into account the Eq. 14, and under the hypotheses that

- the quantity 2·r represents the NMAS of the mixture,
- k_1 represents the sand/bead diameter,
- MTD ≥ k_1,

the Eq. 14 was generalized as follows (see Tab. 4, and Eq. 15) where k_2, α, and β are coefficients to calibrate. Finally, based on the AV expression (Eq. 13), two expressions of MTD can be considered (cf. Eqs. 17 and 18).

Tab. 4. Model generalization.

Parameter	**Unit of measure**	**Equation**	**Equation number**
Mean Texture Depth	mm	$MTD = k_1 + k_2 \cdot AV^{\alpha} \cdot NMAS^{\beta}$	(15)
Air void content	dim.less (%)	$AV = 1 - \frac{Gmb}{Gmm} = 1 - \frac{P_T \cdot \left(\frac{Pag}{Gse} + \frac{Pb}{Gb} \right)}{P_T \cdot \left(\frac{Pag}{Gse} + \frac{Pb}{Gb} + Va \right)} =$ $= \frac{V_T}{V_T} - \frac{1}{V_T} \cdot \left[\frac{Pag}{Gse} + \frac{Pb}{Gb} \right] =$ $= \frac{V_T}{V_T} - \frac{Gmb}{P_T} \cdot \left[\frac{Psand}{Gse_{sand}} + \frac{Pf}{Gse_f} + \frac{Pb}{Gb} \right] =$ $= \frac{V_T}{V_T} - \frac{Gmb}{P_T} \cdot [FV] \cong$ $\cong 1 - k \cdot \frac{Psand}{Gse_{sand}} - k \cdot [FV] \cong k_3 - k_4 \cdot [FV]$ with $k_3 \geq k_4 \cdot [FV]$, with FV stands for filled volume.	(16)
Mean Texture Depth	mm	$MTD = k_1 + k_2 \cdot \left(1 - \frac{Gmb}{Gmm} \right)^{\alpha} \cdot NMAS^{\beta} =$ $= k_1 + k_2 \cdot (k_3 - k_4 \cdot FV)^{\alpha} \cdot NMAS^{\beta}$	(17)
The following equations were investigated:			
Mean Texture Depth	mm	When $k_3 = 0$, $k_4 = -1$, and $\gamma = -\alpha$	

		$MTD = k_1 + \frac{k_2 \cdot NMAS^{\beta}}{FV^{\gamma}}$ where k_2, k_3 and k_4 are compaction dependent.	(18)
Filled volumes Note that the following values were used to derive the filled volumes, FVi (with i=1, …, 8), i.e. Gse_{sand}=2.75; $Gse_{4.75app}$=2.76; $Gse_{4.75}$=2.75; Gse_{filler}=2.93; Gb=1.02.	[dim.less]	$FV1 = \frac{P_{sand}}{Gse_{sand}}$	(19)
		$FV2 = \frac{P_{4.75}}{Gse_{4.75app}}$	(20)
		$FV3 = \frac{P_{4.75} - P_{filler}}{Gse_{4.75}}$	(21)
		$FV4 = \frac{P_{filler}}{Gse_{filler}}$	(22)
		$FV5 = \frac{P_b}{G_b}$	(23)
		$FV6 = \frac{P_{sand}}{Gse_{sand}} + \frac{P_{filler}}{Gse_{filler}} + \frac{P_b}{G_b}$	(24)
		$FV7 = \frac{P_{4.75}}{Gse_{4.75app}} + \frac{P_b}{G_b}$	(25)
		$FV8 = \frac{P_{4.75} - P_{filler}}{Gse_{4.75}} + \frac{P_{filler}}{Gse_{filler}} + \frac{P_b}{G_b}$	(26)

By referring to equations 17 and 18, note that the sphere packing model yields a solution where MTD is linearly proportional to AV. On the other hand, due to its intrinsic approximations solutions where MTD is proportional to the power of AV have demonstrated to increase the percentage of explained variance. Furthermore, based on the equations above, under the assumptions of the sphere packing model, it is:

$$k_3 - k_4 \cdot FV = a \cdot (1 - b \cdot FV), \tag{27}$$

and

$$(k_3 - k_4 \cdot FV)^{\alpha} = c \cdot (1 - d \cdot FV)^{\alpha}. \tag{28}$$

The expressions above may have drawbacks in terms of optimisation and rationale behind.

Indeed, both 1-b·FV and 1-d·FV must be positive (as AV) and this may raise issues in terms of optimisation when considering the power. Furthermore, the expressions (1-b·FV) and (1-d·FV) do not comply with the rationale behind the concept of AV, because FV focuses on the filling material and

does not consider the remaining part of the volume filled by coarse aggregate. In order to overcome the issues above, let us introduce the factor $1/FV^{\alpha}$ as an alternative to $c\cdot(1-d\cdot FV)^{\alpha}$.

Figure 5 illustrates the transition from AV to k_3-$k_4\cdot FV$ to $1/FV^{\gamma}$.

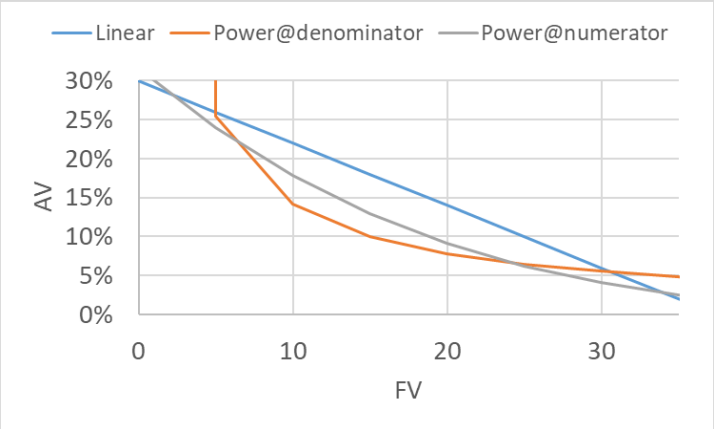

Figure 5. Transition from AV to k_3-$k_4\times FV$ to $1/FV^{\gamma}$.

Equations 19 to 26 refer to the concept of filling volume as the fine part of the mixture (e.g., sand and bitumen) free to flow and fill the voids left from the coarse portion of aggregate, e.g., the sphere of the sphere packing model, where FV3+FV4+FV5=FV8. Table 5 illustrates how the eight indicators above perform for the data set RE. Note that the highest values are often the ones that correspond to dense-graded mixtures, while the lowest are usually the ones that pertain to open-graded mixtures.

Tab. 5. Filled volumes (FV) related to the data set RE.

Mix	**DGFCs**												
Ref.	CIRS [31]						ANAS [32]						
Tentative name	CIRS-DGFC-A	CIRS-DGFC-B	CIRS-DGFC -C	CIRS-DGFC(m)-A	CIRS-DGFC(m)-B	CIRS-DGFC(m)-C	ANAS-DGFC-A	ANAS-DGFC-B	ANAS-DGFC(ms)-A	ANAS-DGFC(ms)-B	ANAS-DGFC(mh)-A	ANAS-DGFC(mh)-B	ANAS-DGFC-A+Foam Clay
FV1	8.5	8.5	10.4	8.5	8.5	10.4	8.5	9.8	8.5	9.8	8.5	9.8	8.5
FV2	17.2	18.1	19.9	17.2	18.1	19.9	17.8	19.6	17.8	19.6	17.8	19.6	17.8
FV3	14.4	15.3	17.1	14.4	15.3	17.1	14.9	16.7	14.9	16.7	14.9	16.7	14.9
FV4	2.7	2.7	2.7	2.7	2.7	2.7	2.7	2.7	2.7	2.7	2.7	2.7	2.7

FV5	5.2	5.4	5.6	5.2	5.4	5.6	5.2	5.2	5.2	5.2	5.2	5.2	6.0
FV6	16.5	16.7	18.7	16.5	16.7	18.7	16.5	17.7	16.5	17.7	16.5	17.7	17.3
FV7	22.4	23.5	25.5	22.4	23.5	25.5	22.9	24.8	22.9	24.8	22.9	24.8	23.7
FV8	22.3	23.4	25.4	22.3	23.4	25.4	22.8	24.7	22.8	24.7	22.8	24.7	23.6

Mix	**OGFCs**			**M**			**S**		
Ref.	CIRS [31]	ANAS [32]	ANAS [32]	CIRS [31]	ANAS [32]	ANAS [32]	CIRS [31]	CIRS [31]	CIRS [31]
Tentative name	CIRS-OGFC	ANAS-OGFC	ANAS-OGFC+ +Foam Clay	CIRS-M	ANAS-M-HOT	ANAS-M-COLD	CIRS-S 0/12	CIRS-S 0/8	CIRS-S 0/5
FV1	3.3	1.1	1.1	4.5	14.7	12.7	5.5	4.7	4.0
FV2	7.2	4.5	4.0	9.1	29.0	23.6	15.4	14.1	34.4
FV3	5.1	2.4	1.8	6.4	26.4	20.9	11.8	10.5	30.9
FV4	2.0	2.0	2.0	2.6	2.6	2.6	3.4	3.4	3.4
FV5	5.4	5.2	5.7	5.4	5.2	7.4	6.9	6.9	7.4
FV6	10.7	8.3	8.8	12.5	22.5	22.6	15.7	15.0	14.8
FV7	12.6	9.7	9.7	14.5	34.2	30.9	22.3	21.0	41.8
FV8	12.5	9.6	9.6	14.3	34.1	30.8	22.1	20.8	41.7

Symbols. See Tables 1.

4. Experiments

In order to assess mean texture depth *(MTD)* variability in the domain of low-Nominal Maximum Aggregate Size (*NMAS)* mixtures, fifty-two specimens were designed, produced, and tested (data set EX, Task 3). Tables 6 and 7 report the standards related to the methods used in this study.

Tab. 6. Mix design methods applied and tests carried out on the specimens.

Method	**Standard**
Superpave Giratory Compactor method	AASHTO T-312 [44], EN 12697-31 [45]
Marshall method	ASTM D6926-20 [46] , EN 12697-30 [47]

Tab. 7. Methods, indicators, and standards taken into account in this study.

Test	**Indicator**	**Standard**
Sand patch method	Mean Texture Depth (*MTD*)	ASTM E965 [48], and EN 13036-1 [33,49]
Corelok machine	Bulk Specific Gravity (*Gmb)*, and AV	AASHTO T-331 [50], and ASTM D6752-09 [51]

Figure 6 depicts the main devices used. In particular, Figs. 6.a and 6.b show the two devices used to produce the specimens, i.e. the Superpave Gyratory compactor and the Marshall compactor, respectively. At the same time, Fig. 6.c shows the devices used to estimate the air void content and the Gmb of the specimens (cf. Tab. 7), i.e. the corelok machine (Fig. 6.c.1), the weight scale with on top the plastic bag used to seal the specimens (Fig. 6.c.2), and the specimens sealed in the plastic bag by the corelok machine (Fig. 6.c.3). Finally, Fig. 6.d shows one specimen before (Fig. 6.d.1) and after (Fig. 6.d.2) the application of the sand patches method that was used to estimate the macrotexture of the specimens (in terms of mean texture depth, MTD). Figure 7 shows the gradation curves of the mixtures created in laboratory.

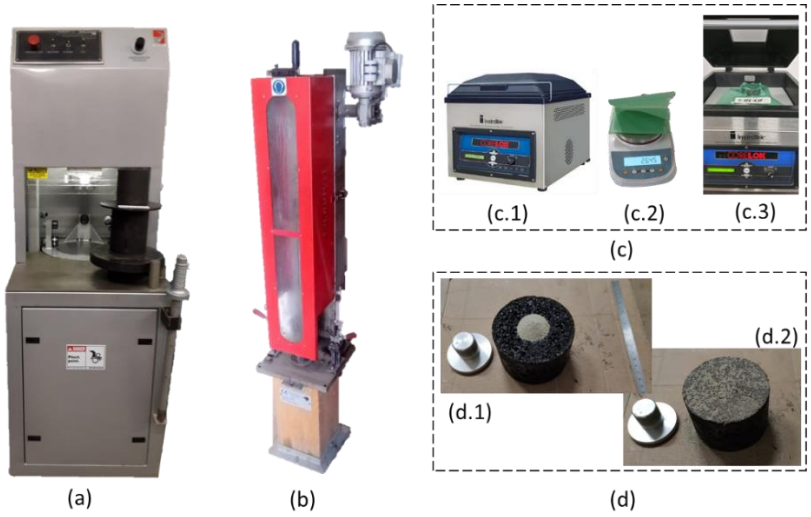

Figure 6. Devices used to produce (i.e., a: Superpave Gyratory Compactor, and b: Marshall compactor) and tests (i.e., c: Corelok machine, and d: devices used to apply the sand patch method) the specimens used in this study.

Table 8 shows ranges and variations of the parameters related to the data set EX, which were derived carrying out the tests listed in Tab. 7.

Tab. 8. Variance of the main parameters related to the data sets EX and LI.

Data set	**Descriptive statistic**	**Pb (%)**	**AV (%)**	**MTD [mm]**	**NMAS [mm]**	**P_{sand} (%)**	**$P_{4.75}$ (%)**	**P_{filler} (%)**
EX	**min**	3.0	0.1	0.1	5.6	14.7	58.2	6.4
EX	**max**	7.2	15.8	0.9	7.2	53.1	85.6	11.5
EX	**mean**	5.5	4.9	0.4	6.6	26.4	71.1	8.8
EX	**st.dev.**	1.14	3.59	0.23	0.56	14.02	10.74	1.46

LI	**min**	4.0	2.2	0.2	2.5	3.5	13.3	2.0
LI	**max**	9.0	26.5	4.5	17.5	71.0	100.0	16.0
LI	**mean**	5.5	11.7	1.5	11.7	23.9	49.1	5.3
LI	**st.dev.**	1.03	8.03	1.25	4.03	16.00	24.03	3.50
Symbols. See tables above.								

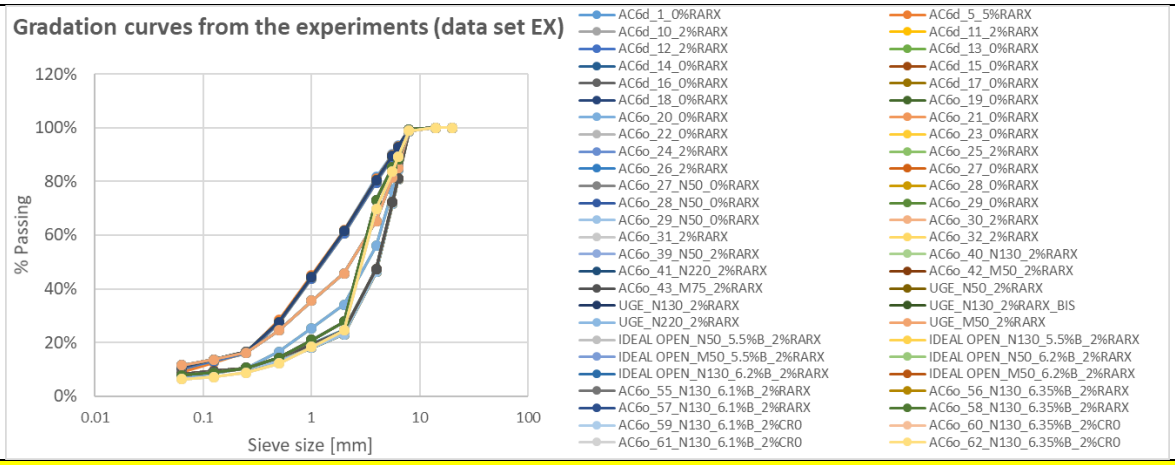

(a)

Mix Name	Mix #	Name	#
AC6d_1_0%RARX	1	AC6o_31_2%RARX	27
AC6d_5_5%RARX	2	AC6o_32_2%RARX	28
AC6d_10_2%RARX	3	AC6o_39_N50_2%RARX	29
AC6d_11_2%RARX	4	AC6o_40_N130_2%RARX	30
AC6d_12_2%RARX	5	AC6o_41_N220_2%RARX	31
AC6d_13_0%RARX	6	AC6o_42_M50_2%RARX	32
AC6d_14_0%RARX	7	AC6o_43_M75_2%RARX	33
AC6d_15_0%RARX	8	UGE_N50_2%RARX	34
AC6d_16_0%RARX	9	UGE_N130_2%RARX	35
AC6d_17_0%RARX	10	UGE_N130_2%RARX_BIS	36
AC6d_18_0%RARX	11	UGE_N220_2%RARX	37
AC6o_19_0%RARX	12	UGE_M50_2%RARX	38
AC6o_20_0%RARX	13	IDEAL OPEN_N50_5.5%B_2%RARX	39
AC6o_21_0%RARX	14	IDEAL OPEN_N130_5.5%B_2%RARX	40
AC6o_22_0%RARX	15	IDEAL OPEN_M50_5.5%B_2%RARX	41
AC6o_23_0%RARX	16	IDEAL OPEN_N50_6.2%B_2%RARX	42
AC6o_24_2%RARX	17	IDEAL OPEN_N130_6.2%B_2%RARX	43
AC6o_25_2%RARX	18	IDEAL OPEN_M50_6.2%B_2%RARX	44
AC6o_26_2%RARX	19	AC6o_55_N130_6.1%B_2%RARX	45
AC6o_27_0%RARX	20	AC6o_56_N130_6.35%B_2%RARX	46
AC6o_27_N50_0%RARX	21	AC6o_57_N130_6.1%B_2%RARX	47
AC6o_28_0%RARX	22	AC6o_58_N130_6.35%B_2%RARX	48
AC6o_28_N50_0%RARX	23	AC6o_59_N130_6.1%B_2%CR0	49
AC6o_29_0%RARX	24	AC6o_60_N130_6.35%B_2%CR0	50
AC6o_29_N50_0%RARX	25	AC6o_61_N130_6.1%B_2%CR0	51
AC6o_30_2%RARX	26	AC6o_62_N130_6.35%B_2%CR0	52

(b)

Mix	% Passing													Mix	% Passing												
#	20.0	16.0	14.0	10.0	8.0	6.3	4.0	2.0	1.0	0.50	0.25	0.125	0.063	#	20.0	16.0	14.0	10.0	8.0	6.3	4.0	2.0	1.0	0.50	0.25	0.125	0.063
1	100	100	99	93	90	82	62	45	28	17	13	9	0	27	100	100	99	81	72	47	25	19	14	11	9	8	0
2	100	100	99	93	90	81	62	45	28	16	13	9	0	28	100	100	99	81	72	47	25	19	14	11	9	8	0
3	100	100	99	93	89	80	60	44	27	16	13	10	0	29	100	100	99	81	72	47	25	19	14	11	9	8	0
4	100	100	99	93	89	80	60	44	27	16	13	10	0	30	100	100	99	81	72	47	25	19	14	11	9	8	0
5	100	100	99	93	89	80	60	44	27	16	13	10	0	31	100	100	99	81	72	47	25	19	14	11	9	8	0
6	100	100	99	93	90	80	61	45	28	17	14	11	0	32	100	100	99	81	72	47	25	19	14	11	9	8	0
7	100	100	99	93	90	80	61	45	28	17	14	11	0	33	100	100	99	81	72	47	25	19	14	11	9	8	0
8	100	100	99	93	90	80	61	45	28	17	14	11	0	34	100	100	99	85	81	65	46	36	25	16	14	12	0
9	100	100	99	93	90	80	61	45	28	17	14	11	0	35	100	100	99	85	81	65	46	36	25	16	14	12	0
10	100	100	99	93	90	80	61	45	28	17	14	11	0	36	100	100	99	85	81	65	46	36	25	16	14	12	0
11	100	100	99	93	90	80	61	45	28	17	14	11	0	37	100	100	99	85	81	65	46	36	25	16	14	12	0
12	100	100	99	84	77	56	34	25	17	10	9	7	0	38	100	100	99	85	81	65	46	36	25	16	14	12	0
13	100	100	99	84	77	56	34	25	17	10	9	7	0	39	100	100	99	88	85	73	28	21	14	11	9	8	0
14	100	100	99	81	72	46	23	18	13	10	9	8	0	40	100	100	99	88	85	73	28	21	14	11	9	8	0
15	100	100	99	81	72	46	23	18	13	10	9	8	0	41	100	100	99	88	85	73	28	21	14	11	9	8	0
16	100	100	99	81	72	46	23	18	13	10	9	8	0	42	100	100	99	88	85	73	28	21	14	11	9	8	0
17	100	100	99	81	72	47	25	19	14	11	9	8	0	43	100	100	99	88	85	73	28	21	14	11	9	8	0
18	100	100	99	81	72	47	25	19	14	11	9	8	0	44	100	100	99	88	85	73	28	21	14	11	9	8	0
19	100	100	99	81	72	47	25	19	14	11	9	8	0	45	100	100	99	88	85	73	28	21	14	11	9	8	0
20	100	100	99	81	72	46	23	18	13	10	9	8	0	46	100	100	99	88	85	73	28	21	14	11	9	8	0
21	100	100	99	81	72	46	23	18	13	10	9	8	0	47	100	100	99	88	85	73	28	21	14	11	9	8	0
22	100	100	99	81	72	46	23	18	13	10	9	8	0	48	100	100	99	88	85	73	28	21	14	11	9	8	0
23	100	100	99	81	72	46	23	18	13	10	9	8	0	49	100	100	99	89	84	70	25	18	12	9	7	6	0
24	100	100	99	81	72	46	23	18	13	10	9	8	0	50	100	100	99	89	84	70	25	18	12	9	7	6	0
25	100	100	99	81	72	46	23	18	13	10	9	8	0	51	100	100	99	89	84	70	25	18	12	9	7	6	0
26	100	100	99	81	72	47	25	19	14	11	9	8	0	52	100	100	99	89	84	70	25	18	12	9	7	6	0

(c)

Figure 7. Aggregate gradations (data set EX): a) Gradation curves; b) Names and corresponding numbers; c) Percentage passing.

5. Model implementation

Based on the studies and the experiments carried out, model implementation (Task 4) was performed. For the purpose of assessing if the equations above have the ability to predict MTD, they were first calibrated and after validated, taking into account (cf. Figs. 1 and 8): 1) Three different data sets (LI, EX, RE) and their combinations, giving seven possible data sets (LI, EX, RE, LI ∪ EX, LI ∪ RE, EX ∪ RE, LI ∪ EX ∪ RE). 2) Two main equations to analyse, i.e., Eqs. 17 and 18. 3) Eight main expressions for FVi (cf. Tab. 4). 4) Overall $7 \cdot 2 \cdot 8 = 112$ possible combinations. Figure 8 summarises these efforts.

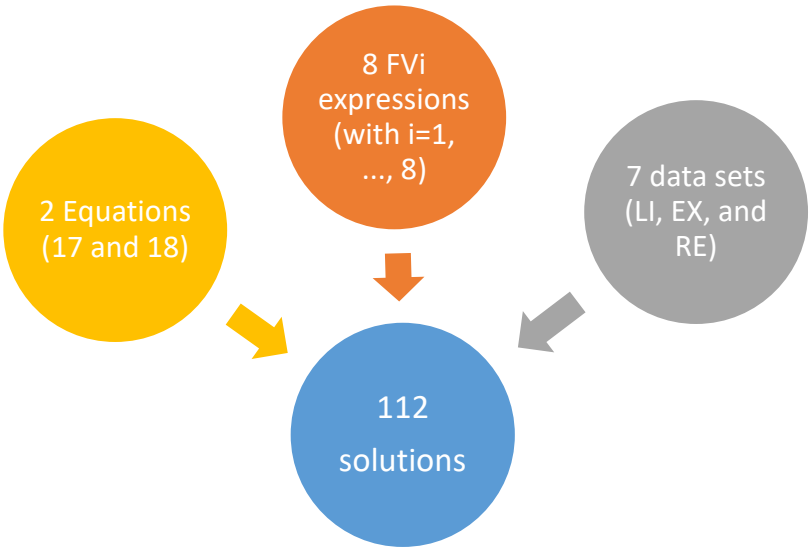

Phase	Eqs.	Indicators	Data set	Tables	Figs
Calibration	17,18	FV1, …, FV8	LI, EX, RE, LI ∪ EX, LI ∪ RE, EX ∪ RE, LI ∪ EX	9-12	9-11
	18	FV2, FV3, FV7, FV8	LI, EX, RE, LI ∪ EX		
Validation	18(LI)	FV2, FV3, FV7, FV8	EX, RE, RE*	13-16	13,14

Figure 8. Framework of the study (see Fig. 1).

Tables 9-12 refer to calibration (Eqs. 17 and 18, data set LI, EX, LI ∪ EX). Attention was preliminary focused on Eqs. 17 and 18, and on FVi. The calibration of Eq. 17 with different data sets underwent multiple issues because of the term $(k_3\text{-}k_4 \cdot FV)^{\alpha}$. Issues were partly solved by forcing factors, but, overall, Eq. 17 yielded lower percentages of explained variance (see Table 9, $R^2 < 0.84$). Indeed, after several attempts, k_1, k_3, and α were imposed equal to the values that allow Eq. 17 fitting, i.e. 0.2, 1, and 1, respectively. For FVi, all the expressions resulted in quite sound results but only four out of eight expressions were selected because of slight improvements of R-square and/or their ability to explain particular types of mixtures (e.g., FV8 for SMAs). For data set, the data set RE (requirements) was considered less appropriate than LE and EX because in it a lower number of mixture types are considered, and because they refer to requirements and not to real mixtures. Based on the above, Eq. 18 and the selected four FVi were used for the calibration, using three data sets, i.e., LI (see Tab. 9), EX (see Tab. 10), LI ∪ EX (see Tab. 11).

For validation, Eq. 18 (calibrated for LI) and the selected four FVi were validated against the data sets EX (Table 13) or RE (Tabs. 14-16). Tables 9 and 10 report the results obtained using the Eqs. 17 and

18, respectively. Figures 9 and 10 report the results obtained using the equations 17 considering the intercept or using the intercept equal to zero, respectively.

Tab. 9. Model calibration (Eq. 17 and data set LI ∪ EX).

Sol. 1	**Using FV2=P4.75/Gse$_{4.75app}$**									
-	**k_1**	**k_2**	**k_3**	**k_4**	**α of (1-k_4×FV)**	**β of NMAS**	**Error**	**Pearson**	**R^2**	**ΔR^2**
1.1	0.20	0.036	1.0	0.040	1.0	1.739	29.926	0.910	82.75%	-0.677%
Sol. 2	**FV3=(P4.75-Pfiller)/Gse$_{4.75}$**									
-	**k_1**	**k_2**	**k_3**	**k_4**	**α of (1-k_3×FV)**	**β of NMAS**	**Error**	**Pearson**	**R^2**	**ΔR^2**
2.1	0.20	0.069	1.0	0.043	1.0	1.470	32.831	0.894	79.85%	-3.579%
Sol. 3	**Using FV8= [(P4.75-Pfiller)/Gse$_{4.75}$]+(Pfiller/Gse$_{filler}$)+(Pb/Gb)**									
-	**k_1**	**k_2**	**k_3**	**k_4**	**α of (1-k_3×FV)**	**β of NMAS**	**Error**	**Pearson**	**R^2**	**ΔR^2**
3.1	0.20	0.022	1.0	0.034	1.0	1.980	30.119	0.913	83.35%	-0.075%
Sol. 4	**Using FV7= (P4.75/Gse$_{4.75app}$)+(Pb/Gb)**									
-	**k_1**	**k_2**	**k_3**	**k_4**	**α of (1-k_3×FV)**	**β of NMAS**	**Error**	**Pearson**	**R^2**	**ΔR^2**
4.1	0.20	0.022	1.0	0.033	1.0	1.990	30.026	0.913	83.43%	0.000%
Symbols. Sol.=Solution; ΔR^2=Decrease of explained variance calculated considering the four reported solutions (i.e., 1.1-4.1); Grey cells=Values imposed before the iteration.										

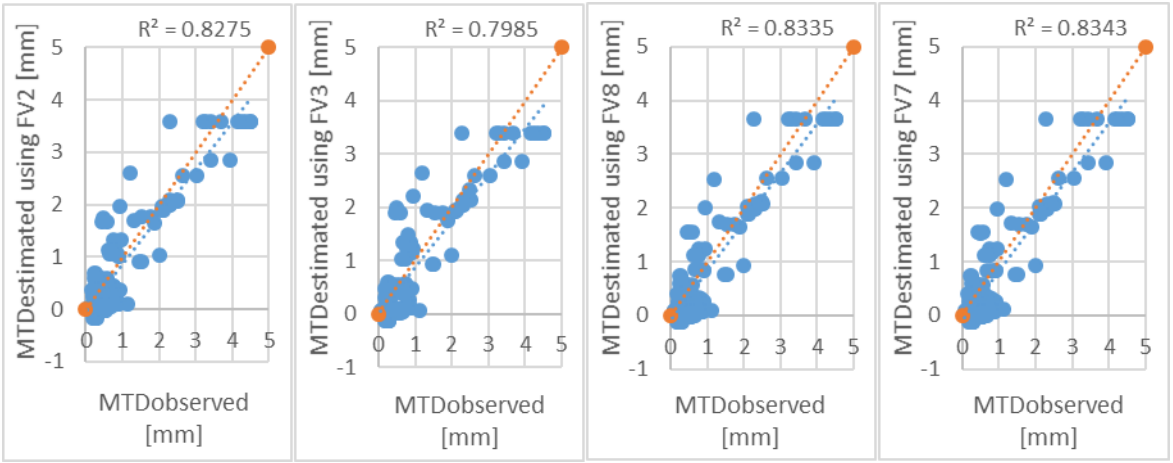

(a) (b) (c) (d)

Figure 9. MTD observed (data set LI ∪ EX) vs. MTD estimated through Eq. 17 (cf. Tab. 4).

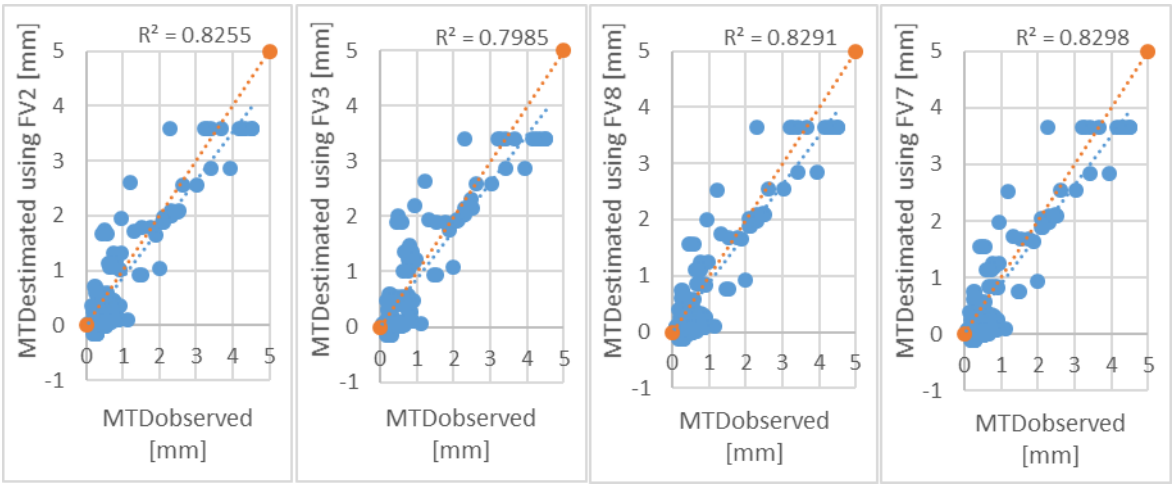

(a) (b) (c) (d)

Figure 10. MTD observed (data set LI ∪ EX) vs. MTD estimated through Eq. 17 (cf. Tab. 4) with the intercept=0.

Note that negative values (i.e., with no physical meaning) were obtained using the Eq. 17, when considering Eq. 17 without forcing α.

Tab. 10. Model calibration (Eq. 18 and data set LI).

Sol. 1	**Using FV2=P4.75/Gse$_{4.75app}$**							
-	**k_1**	**k_2**	**β of NMAS**	**γ of FV**	**Error**	**Pearson**	**R^2**	**ΔR^2**
1.1	-2.206	22.628	-0.121	0.575	14.51	0.933	87.14%	0.0%
1.2	0.000	14.130	0.262	1.152	15.557	0.929	86.24%	-0.9%
1.3	0.000	0.002	3.396	1.009	40.045	0.857	73.46%	-13.7%
1.4	**0.200**	**9.105**	**0.478**	**1.266**	**16.010**	**0.927**	**85.87%**	**-1.3%**
1.5	0.200	0.002	3.472	1.152	32.808	0.869	75.45%	-11.7%
Sol. 2	**FV3=(P4.75-Pfiller)/Gse$_{4.75}$**							
-	**k1**	**k2**	**β of NMAS**	**γ of FV**	**Error**	**Pearson**	**R^2**	**ΔR^2**
2.1	-4.764	17.923	-0.086	0.332	15.599	0.928	86.18%	0.0%
2.2	0.000	7.797	0.336	1.047	17.467	0.920	84.55%	-1.6%
2.3	0.000	0.002	3.348	1.028	39.529	0.862	74.35%	-11.8%
2.4	**0.200**	**3.976**	**0.624**	**1.146**	**17.870**	**0.918**	**84.21%**	**-2.0%**
2.5	0.200	0.002	3.416	1.174	32.082	0.874	76.34%	-9.8%
Sol. 3	**Using FV8= [(P4.75-Pfiller)/Gse$_{4.75}$]+(Pfiller/Gse$_{_filler}$)+(Pb/Gb)**							
-	**k_1**	**k_2**	**β of NMAS**	**γ of FV**	**Error**	**Pearson**	**R^2**	**ΔR^2**
3.1	0.167	54.196	0.553	1.791	15.160	0.930	86.57%	0.0%
3.2	0.000	74.197	0.323	1.643	15.222	0.930	86.51%	-0.1%

3.3	0.000	0.002	3.958	1.417	43.275	0.849	72.04%	-14.5%
3.4	**0.200**	**50.533**	**0.605**	**1.825**	**15.164**	**0.930**	**86.56%**	**0.0%**
3.5	0.200	0.002	4.119	1.625	35.354	0.861	74.12%	-12.5%
Sol. 4	**Using FV7= (P4.75/Gse$_{4.75app}$)+(Pb/Gb)**							
-	**k_1**	**k_2**	**β of NMAS**	**γ of FV**	**Error**	**Pearson**	**R^2**	**ΔR^2**
4.1	0.165	56.392	0.545	1.796	15.113	0.931	86.61%	0.0%
4.2	0.000	76.283	0.320	1.648	15.176	0.930	86.55%	-0.1%
4.3	0.000	0.002	3.956	1.413	43.273	0.849	72.00%	-14.6%
4.4	**0.200**	**52.437**	**0.599**	**1.831**	**15.117**	**0.931**	**86.60%**	**0.0%**
4.5	0.200	0.002	4.117	1.620	35.373	0.861	74.07%	-12.5%
Symbols. See Tab. 9.								

Tab. 11. Model calibration (Eq. 18 and data set EX).

Sol. 1	**Using FV2=P4.75/Gse$_{4.75app}$**							
-	**k_1**	**k_2**	**β of NMAS**	**γ of FV**	**Error**	**Pearson**	**R^2**	**ΔR^2**
1.1	-0.986	0.347	0.771	0.016	2.16	0.426	18.14%	0.0%
1.2	0.000	0.004	2.445	0.024	2.205	0.409	16.73%	-1.4%
1.3	0.000	0.002	2.717	-0.066	2.207	0.407	16.58%	-1.6%
1.4	**0.200**	**0.0001**	**4.257**	**0.062**	**2.252**	**0.389**	**15.15%**	**-3.0%**
1.5	0.200	0.002	3.275	0.455	2.257	0.387	15.01%	-3.1%
Sol. 2	**FV3=(P4.75-Pfiller)/Gse$_{4.75}$**							
-	**k_1**	**k_2**	**β of NMAS**	**γ of FV**	**Error**	**Pearson**	**R^2**	**ΔR^2**
2.1	-0.830	0.138	1.040	-0.078	2.162	0.427	18.25%	0.0%
2.2	0.000	0.005	2.384	0.042	2.208	0.408	16.61%	-1.6%
2.3	0.000	0.002	2.661	-0.104	2.201	0.412	16.96%	-1.3%
2.4	**0.200**	**0.00001**	**4.962**	**-0.260**	**2.248**	**0.392**	**15.38%**	**-2.9%**
2.5	0.200	0.002	2.115	-0.248	2.387	0.418	17.45%	-0.8%
Sol. 3	**Using FV8= [(P4.75-Pfiller)/Gse$_{4.75}$]+(Pfiller/Gse$_{filler}$)+(Pb/Gb)**							
-	**k_1**	**k_2**	**β of NMAS**	**γ of FV**	**Error**	**Pearson**	**R^2**	**ΔR^2**
3.1	-0.990	0.099	1.068	-0.186	2.125	0.443	19.63%	0.0%
3.2	0.000	0.013	2.088	0.126	2.229	0.399	15.96%	-3.7%
3.3	0.000	0.002	2.528	-0.169	2.187	0.423	17.89%	-1.7%
3.4	**0.200**	**0.000001**	**5.436**	**-0.730**	**2.213**	**0.415**	**17.21%**	**-2.4%**
3.5	0.200	0.002	1.433	-0.597	2.512	0.348	12.14%	-7.5%
Sol. 4	**Using FV7= (P4.75/Gse$_{4.75app}$)+(Pb/Gb)**							
-	**k_1**	**k_2**	**β of NMAS**	**γ of FV**	**Error**	**Pearson**	**R^2**	**ΔR^2**
4.1	-0.993	0.103	1.058	-0.182	2.127	0.442	19.56%	0.0%
4.2	0.000	0.012	2.121	0.128	2.228	0.399	15.95%	-3.6%
4.3	0.000	0.002	2.532	-0.167	2.188	0.422	17.84%	-1.7%
4.4	**0.200**	**0.0000002**	**5.777**	**-0.832**	**2.211**	**0.413**	**17.08%**	**-2.5%**
4.5	0.200	0.002	1.732	-0.429	2.436	0.431	18.59%	-1.0%
Symbols. See Tab. 9.								

Tab. 12. Model calibration (Eq. 18 and data set LI ∪ EX).

Sol. 1	**Using FV2=P4.75/Gse$_{4.75app}$**							
-	**k_1**	**k_2**	**β of NMAS**	**γ of FV**	**Error**	**Pearson**	**R^2**	**ΔR^2**
1.1	-0.440	15.893	0.961	0.134	17.978	0.937	87.86%	0.000%
1.2	0.000	8.777	1.158	0.442	18.260	0.936	87.68%	-0.182%
1.3	0.000	0.002	0.951	3.356	49.826	0.878	77.17%	-10.683%
1.4	**0.200**	**4.792**	**1.284**	**0.728**	**18.854**	**0.934**	**87.32%**	**-0.542%**
1.5	0.200	0.002	1.122	3.450	37.197	0.889	79.00%	-8.858%
Sol. 2	**FV3=(P4.75-Pfiller)/Gse$_{4.75}$**							
-	**k_1**	**k_2**	**β of NMAS**	**γ of FV**	**Error**	**Pearson**	**R^2**	**ΔR^2**
2.1	-0.392	8.901	0.890	0.233	20.099	0.930	86.43%	0.000%
2.2	0.000	4.368	1.051	0.554	20.274	0.929	86.31%	-0.114%
2.3	0.000	0.002	0.969	3.310	49.349	0.882	77.81%	-8.617%
2.4	**0.200**	**2.086**	**1.167**	**0.876**	**20.701**	**0.928**	**86.05%**	**-0.379%**
2.5	0.200	0.002	1.142	3.396	36.490	0.892	79.64%	-6.784%
Sol. 3	**Using FV8= [(P4.75-Pfiller)/Gse$_{4.75}$]+(Pfiller/Gse$_{filler}$)+(Pb/Gb)**							
-	**k_1**	**k_2**	**β of NMAS**	**γ of FV**	**Error**	**Pearson**	**R^2**	**ΔR^2**
3.1	0.180	34.023	1.819	0.749	17.908	0.938	87.90%	0.000%
3.2	0.000	50.894	1.642	0.462	18.137	0.937	87.76%	-0.142%
3.3	0.000	0.002	1.345	3.893	53.934	0.872	76.07%	-11.834%
3.4	**0.200**	**32.057**	**1.843**	**0.790**	**17.912**	**0.938**	**87.90%**	**-0.002%**
3.5	0.200	0.002	1.589	4.087	40.135	0.883	77.90%	-10.004%
Sol. 4	**Using FV7= (P4.75/Gse$_{4.75app}$)+(Pb/Gb)**							
-	**k_1**	**k_2**	**β of NMAS**	**γ of FV**	**Error**	**Pearson**	**R^2**	**ΔR^2**
4.1	0.178	35.006	1.821	0.742	17.856	0.938	87.94%	0.000%
4.2	0.000	52.538	1.647	0.457	18.079	0.937	87.80%	-0.139%
4.3	0.000	0.002	1.341	3.891	53.925	0.872	76.04%	-11.896%
4.4	**0.200**	**32.945**	**1.846**	**0.785**	**17.861**	**0.938**	**87.94%**	**-0.003%**
4.5	0.200	0.002	1.584	4.085	40.150	0.882	77.87%	-10.068%
Symbols. See Tab. 9.								

Among all the solutions of Eq. 18 reported in the table above, the solutions 1.4, 2.4, 3.4, and 4.4 were used to derive the following figures (i.e., Figs. 11 and 12), which show the accuracy of the proposed model ($R^2 \approx 0.88$).

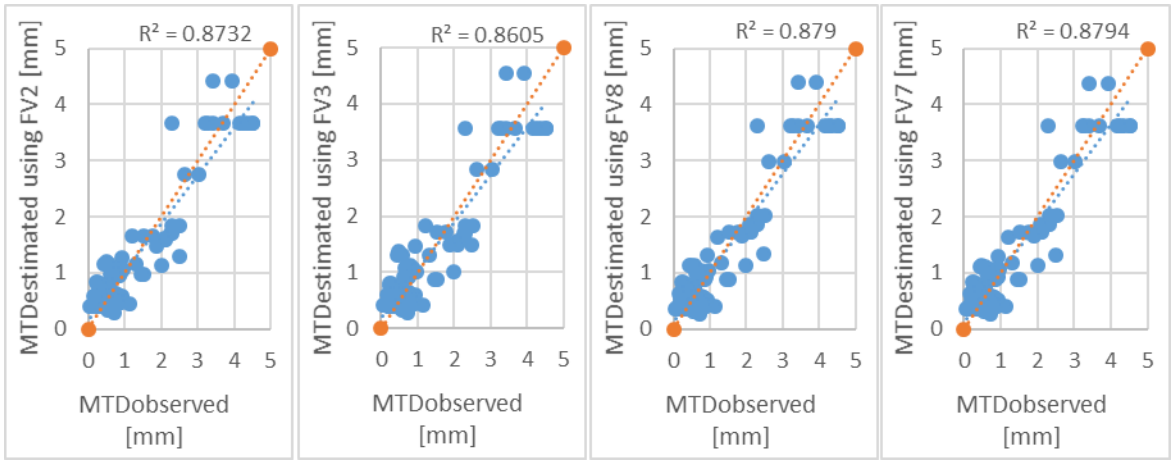

(a) (b) (c) (d)

Figure 11. MTD observed (data set LI ∪ EX) vs. MTD estimated through Eq. 18 (cf. 1.4, 2.4, 3.4, and 4.4 in Tab. 12).

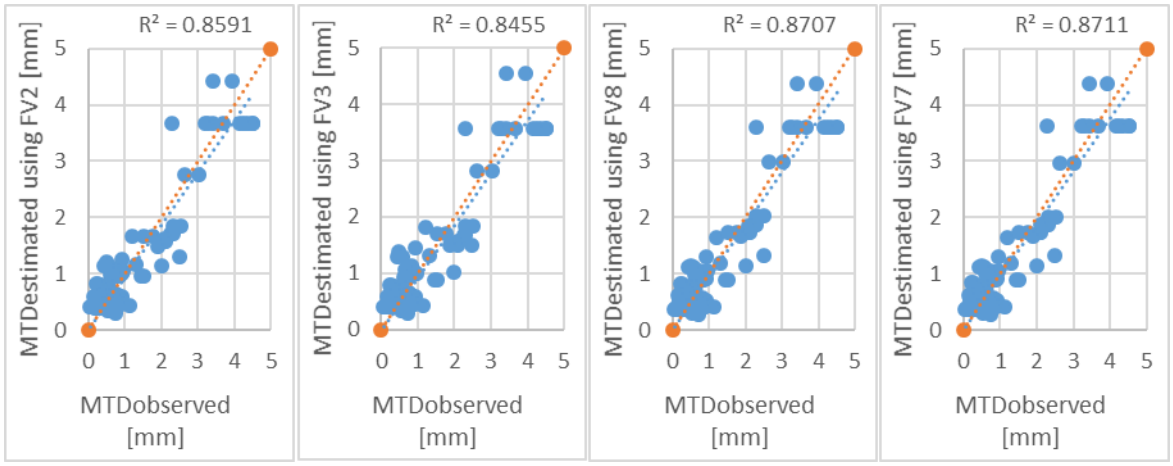

(a) (b) (c) (d)

Figure 12. MTD observed (data set LI ∪ EX) vs. MTD estimated through Eq. 18 (cf. 1.4, 2.4, 3.4, and 4.4 in Tab. 12) with the intercept=0.

Overall, for calibration, it is observed that:

- When the Eq. 18 was applied on LI (cf. Tab. 10), R^2 ranged between 84.2% and 86.6%.
- When the Eq. 18 was applied on EX (cf. Tab. 11), R^2 ranged between 15.1% and 17.2%.
- When the Eq. 18 was applied on LI ∪ EX (cf. Tab. 12), R^2 ranged between 86.1% and 87.9%.

5.1 Model validation

A. Data set of validation: EX

Tables 13 and 14 report the results of the model validation (Eq. 18). In Tab. 13, the coefficients (k_1, k_2, β, and γ) calibrated for LI are used together with the four most efficient FVi (i.e., FV2, FV3, F8, and FV7) to estimate MTD of the data set EX.

Tab. 13. Model validation (Eq. 18) and data set EX calibrated for LI.

Sol. 1	**Using FV2=P4.75/Gse$_{4.75app}$**							
-	**k_1**	**k_2**	**β of NMAS**	**γ of FV**	**Error**	**Pearson**	**R^2**	**ΔR^2**
1.1	-2.206	22.628	-0.121	0.575	5.069	0.334	11.19%	-2.25%
1.2	0.000	14.130	0.262	1.152	3.254	0.350	12.22%	-1.22%
1.3	0.000	0.002	3.396	1.009	9.891	0.367	13.44%	0.00%
1.4	**0.200**	**9.105**	**0.478**	**1.266**	**3.444**	**0.352**	**12.37%**	**-1.06%**
1.5	0.200	0.002	3.472	1.152	4.412	0.361	13.05%	-0.39%
Sol. 2	**FV3=(P4.75-Pfiller)/Gse$_{4.75}$**							
-	**k_1**	**k_2**	**β of NMAS**	**γ of FV**	**Error**	**Pearson**	**R^2**	**ΔR^2**
2.1	-4.764	17.923	-0.086	0.332	11.737	0.285	8.10%	-4.01%
2.2	0.000	7.797	0.336	1.047	3.543	0.315	9.91%	-2.20%
2.3	0.000	0.002	3.348	1.028	9.931	0.348	12.11%	0.00%
2.4	**0.200**	**3.976**	**0.624**	**1.146**	**3.419**	**0.322**	**10.35%**	**-1.76%**
2.5	0.200	0.002	3.416	1.174	4.431	0.342	11.68%	-0.43%
Sol. 3	**Using FV8= [(P4.75-Pfiller)/Gse$_{4.75}$]+(Pfiller/Gse$_{filler}$)+(Pb/Gb)**							
-	**k_1**	**k_2**	**β of NMAS**	**γ of FV**	**Error**	**Pearson**	**R^2**	**ΔR^2**
3.1	0.167	54.196	0.553	1.791	2.978	0.229	5.25%	-3.51%
3.2	0.000	74.197	0.323	1.643	3.148	0.225	5.06%	-3.70%
3.3	0.000	0.002	3.958	1.417	10.738	0.296	8.76%	0.00%
3.4	**0.200**	**50.533**	**0.605**	**1.825**	**2.988**	**0.230**	**5.28%**	**-3.48%**
3.5	0.200	0.002	4.119	1.625	4.795	0.284	8.07%	-0.69%
Sol. 4	**Using FV7= (P4.75/Gse$_{4.75app}$)+(Pb/Gb)**							
-	**k_1**	**k_2**	**β of NMAS**	**γ of FV**	**Error**	**Pearson**	**R^2**	**ΔR^2**
4.1	0.165	56.392	0.545	1.796	5.047	0.204	4.18%	-4.66%
4.2	0.000	76.283	0.320	1.648	3.129	0.227	5.14%	-3.70%
4.3	0.000	0.002	3.956	1.413	10.731	0.297	8.84%	0.00%
4.4	**0.200**	**52.437**	**0.599**	**1.831**	**2.982**	**0.231**	**5.35%**	**-3.48%**
4.5	0.200	0.002	4.117	1.620	4.792	0.285	8.15%	-0.69%
Symbols. See Tab. 9.								

B. Data set of validation: RE (1st trial)

In Tab. 14, the coefficients k_1, k_2, β, and γ calibrated through the data set LI are used to estimate the values of MTD of the data set RE. In this case MTD_{ob} were obtained through the equation (cf. Fig. 13):

$$MTD_{ob} = MTD_{\min} + 0.2 \quad (29)$$

When the Eq. 18 calibrated for the data set LI was applied on the data set EX (cf. Tab. 13), R-square ranged between 5.3% and 12.4%.

Tab. 14. Model validation (Eq. 18) and data set RE calibrated for LI.

Sol. 1	**Using FV2=P4.75/Gse$_{4.75app}$**							
-	**k_1**	**k_2**	**β of NMAS**	**γ of FV**	**Error**	**Pearson**	**R^2**	**ΔR^2**
1.1	-2.206	22.628	-0.121	0.575	42.49	0.893	79.76%	-5.0%
1.2	0.000	14.130	0.262	1.152	40.512	0.904	81.71%	-3.1%
1.3	0.000	0.002	3.396	1.009	11.071	0.909	82.71%	-2.1%
1.4	**0.200**	**9.105**	**0.478**	**1.266**	**38.178**	**0.910**	**82.88%**	**-1.9%**
1.5	0.200	0.002	3.472	1.152	10.280	0.921	84.77%	0.0%
Sol. 2	**FV3=(P4.75-Pfiller)/Gse$_{4.75}$**							
-	**k_1**	**k_2**	**β of NMAS**	**γ of FV**	**Error**	**Pearson**	**R^2**	**ΔR^2**
2.1	-4.764	17.923	-0.086	0.332	79.640	0.884	78.22%	-9.4%
2.2	0.000	7.797	0.336	1.047	123.833	0.872	76.03%	-11.6%
2.3	0.000	0.002	3.348	1.028	33.337	0.935	87.50%	-0.1%
2.4	**0.200**	**3.976**	**0.624**	**1.146**	**121.977**	**0.879**	**77.19%**	**-10.4%**
2.5	0.200	0.002	3.416	1.174	39.079	0.936	87.58%	0.0%
Sol. 3	**Using FV8= [(P4.75-Pfiller)/Gse$_{4.75}$]+(Pfiller/Gse$_{filler}$)+(Pb/Gb)**							
-	**k_1**	**k_2**	**β of NMAS**	**γ of FV**	**Error**	**Pearson**	**R^2**	**ΔR^2**
3.1	0.167	54.196	0.553	1.791	22.234	0.930	86.48%	-0.3%
3.2	0.000	74.197	0.323	1.643	24.130	0.922	85.04%	-1.7%
3.3	0.000	0.002	3.958	1.417	8.313	0.875	76.52%	-10.3%
3.4	**0.200**	**50.533**	**0.605**	**1.825**	**21.863**	**0.932**	**86.78%**	**0.0%**
3.5	0.200	0.002	4.119	1.625	6.600	0.886	78.48%	-8.3%
Sol. 4	**Using FV7= (P4.75/Gse$_{4.75app}$)+(Pb/Gb)**							
-	**k_1**	**k_2**	**β of NMAS**	**γ of FV**	**Error**	**Pearson**	**R^2**	**ΔR^2**
4.1	0.165	56.392	0.545	1.796	21.532	0.930	86.42%	-0.3%
4.2	0.000	76.283	0.320	1.648	23.362	0.922	85.00%	-1.7%
4.3	0.000	0.002	3.956	1.413	8.146	0.873	76.26%	-10.5%
4.4	**0.200**	**52.437**	**0.599**	**1.831**	**21.145**	**0.931**	**86.73%**	**0.0%**
4.5	0.200	0.002	4.117	1.620	6.409	0.885	78.24%	-8.5%
Symbols. See Tab. 9.								

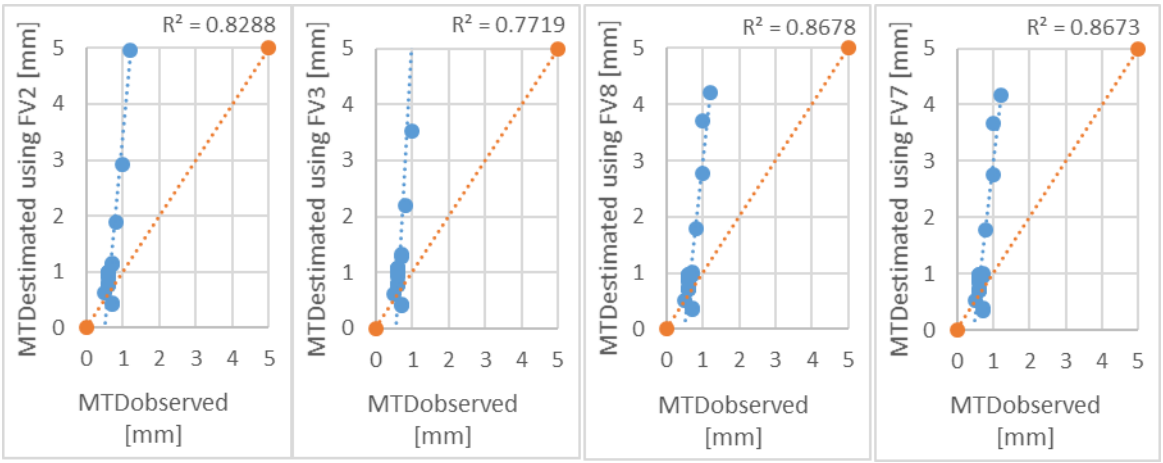

(a) (b) (c) (d)

Figure 13. MTD observed (data set RE) vs. MTD estimated through Eq. 18 (cf. 1.4, 2.4, 3.4, and 4.4 in Tab. 14).

C. Data set of validation: RE (2nd trial)

For validation, it may be observed that when the Eq. 18 calibrated for the data set LI was applied on the data set RE (cf. Tab. 14), R-square ranged between 77.2% and 86.8%. At the same time, Figure 16 shows problems related to the MTD estimated. To this end, for the definition of the parameter MTD, let us suppose that the difference between the average and the minimum value depends on standard deviation and this latter on the expected AV. This seems reasonable because of the need for having a certain distance from the minimum, under the assumption of having sigma/M quite constant. Under these assumptions, having in mind that AV ranges from 3% to about 22% the following tentative formula is here used:

$$\Delta MTD = k \cdot \sigma = m \cdot (AV - 3) + q \tag{30}$$

where m=3/19 and q=0.2. Under these assumptions the scatter plot undergoes an increase of R-square as depicted in Fig. 14. Consequently, by using Eq. 30, the rows related to the parameter MTD of Table 1 change as reported by the following table (Tab. 15). Table 16 reports the results of the proposed model (Eq. 18) validated for the data set RE under the aforementioned hypothesis (Eq. 30).

Tab. 15. Reference requirement for MTD after the application of Eq. 30.

Mix	**DGFCs**												
Ref.	CIRS [31]						ANAS [32]						
Tentative name	CIRS-DGFC-A	CIRS-DGFC-B	CIRS-DGFC -C	CIRS-DGFC(m)-A	CIRS-DGFC(m)-B	CIRS-DGFC(m)-C	ANAS-DGFC-A	ANAS-DGFC-B	ANAS-DGFC(ms)-A	ANAS-DGFC(ms)-B	ANAS-DGFC(mh)-A	ANAS-DGFC(mh)-B	ANAS-DGFC-A+Foam Clay
ΔMTD	0.52	0.52	0.52	0.52	0.52	0.52	0.44	0.44	0.44	0.44	0.44	0.44	0.44
MTDmin	0.40	0.40	0.40	0.40	0.40	0.40	0.40	0.40	0.40	0.40	0.40	0.40	0.40
MTD	0.92	0.92	0.92	0.92	0.92	0.92	0.84	0.84	0.84	0.84	0.84	0.84	0.84

Mix	**OGFCs**			**M**			**S**		
Ref.	CIRS [31]	ANAS [32]	ANAS [32]	CIRS [31]	ANAS [32]	ANAS [32]	CIRS [31]	CIRS [31]	CIRS [31]
Tentative name	CIRS-OGFC	ANAS-OGFC	ANAS-OGFC + Foam Clay	CIRS-M	ANAS-M-HOT	ANAS-M-COLD	CIRS-S 0/12	CIRS-S 0/8	CIRS-S 0/5
ΔMTD	2.41	3.20	3.20	1.62	0.44	-0.27	0.20	0.20	0.20
MTDmin	0.80	1.00	0.80	0.60	0.50	0.30	0.50	0.50	0.50
MTD	3.21	4.20	4.00	2.22	0.94	0.03	0.70	0.70	0.70
Symbols. See Table 1.									

Tab. 16. Model validation (Eq.18) and data set RE (using the Eq. 30) calibrated for LI.

Sol. 1	**Using FV2=P4.75/Gse$_{4.75app}$**							
-	**k_1**	**k_2**	**β of NMAS**	**γ of FV**	**Error**	**Pearson**	**R^2**	**ΔR^2**
1.1	-2.206	22.628	-0.121	0.575	4.56	0.957	91.58%	-0.8%
1.2	0.000	14.130	0.262	1.152	3.936	0.960	92.18%	-0.2%
1.3	0.000	0.002	3.396	1.009	15.092	0.891	79.47%	-13.0%
1.4	**0.200**	**9.105**	**0.478**	**1.266**	**3.396**	**0.961**	**92.43%**	**0.0%**
1.5	0.200	0.002	3.472	1.152	11.258	0.902	81.43%	-11.0%
Sol. 2	**FV3=(P4.75-Pfiller)/Gse$_{4.75}$**							
-	**k_1**	**k_2**	**β of NMAS**	**γ of FV**	**Error**	**Pearson**	**R^2**	**ΔR^2**
2.1	-4.764	17.923	-0.086	0.332	18.636	0.946	89.56%	0.000%
2.2	0.000	7.797	0.336	1.047	42.882	0.933	87.12%	-2.441%
2.3	0.000	0.002	3.348	1.028	11.119	0.928	86.04%	-3.524%
2.4	**0.200**	**3.976**	**0.624**	**1.146**	**41.882**	**0.935**	**87.44%**	**-2.128%**

2.5	0.200	0.002	3.416	1.174	9.650	0.930	86.49%	-3.075%
Sol. 3	**Using FV8= [(P4.75-Pfiller)/Gse$_{4.75}$]+(Pfiller/Gse$_{filler}$)+(Pb/Gb)**							
-	**k_1**	**k_2**	**β of NMAS**	**γ of FV**	**Error**	**Pearson**	**R^2**	**ΔR^2**
3.1	0.167	54.196	0.553	1.791	1.477	0.973	94.62%	0.000%
3.2	0.000	74.197	0.323	1.643	1.387	0.973	94.62%	-0.001%
3.3	0.000	0.002	3.958	1.417	21.252	0.844	71.30%	-23.316%
3.4	**0.200**	**50.533**	**0.605**	**1.825**	**1.509**	**0.973**	**94.59%**	**-0.027%**
3.5	0.200	0.002	4.119	1.625	17.133	0.853	72.77%	-21.846%
Sol. 4	**Using FV7= (P4.75/Gse$_{4.75app}$)+(Pb/Gb)**							
-	**k_1**	**k_2**	**β of NMAS**	**γ of FV**	**Error**	**Pearson**	**R^2**	**ΔR^2**
4.1	0.165	56.392	0.545	1.796	1.523	0.973	94.64%	0.000%
4.2	0.000	76.283	0.320	1.648	1.406	0.973	94.64%	-0.003%
4.3	0.000	0.002	3.956	1.413	21.468	0.843	71.07%	-23.565%
4.4	**0.200**	**52.437**	**0.599**	**1.831**	**1.562**	**0.973**	**94.61%**	**-0.028%**
4.5	0.200	0.002	4.117	1.620	17.356	0.852	72.56%	-22.077%
Symbols. See Tab. 9.								

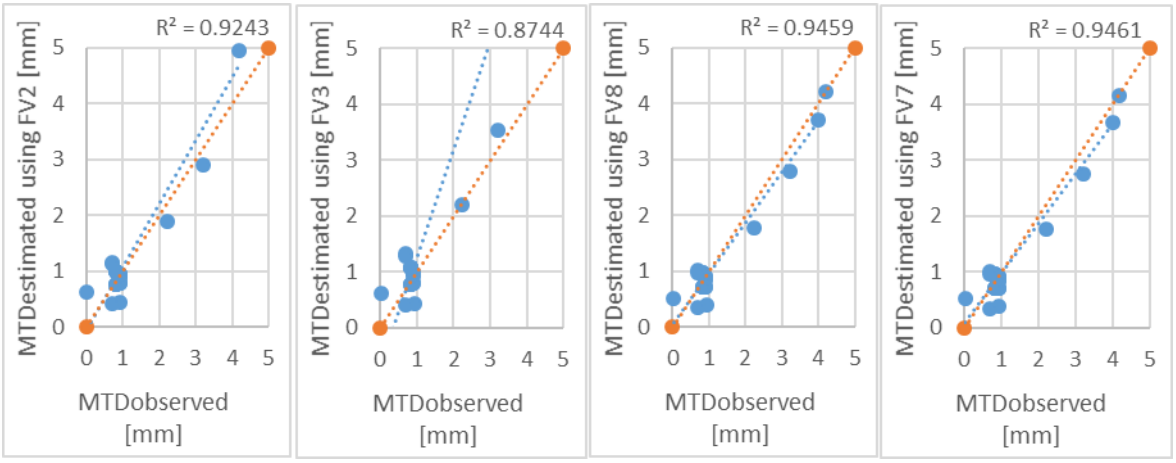

(a) (b) (c) (d)

Figure 14. MTD observed (data set RE using the Eq. 30) vs. MTD estimated through Eq. 18 (cf. 1.4, 2.4, 3.4, and 4.4 in Tab. 16).

In summarizing, the validation of Eq. 18 using the data set RE points out that the distance between the minima MTDs set up in requirements and the expected values cannot be considered constant. On the contrary, it depends on the type of mixture, being higher for open-graded mixtures and vice versa.

6. Conclusions

The surface texture of a pavement affects a number of crucial characteristics, including rolling resistance, friction, noise, and hydroplaning. Technical specifications contribute to increase the number of constrains and variables to consider when designing a low-noise bituminous mixtures. For this reason, the objectives of this study were confined into the modelling and implementation of algorithms to predict mean texture depth (MTD) at a design stage.

Results demonstrate that Nominal Maximum Aggregate Size (NMAS) and filling volume (FV) can explain up to 88% of MTD variance and that using simplified expressions for FV, such as the percentage passing at 4.75 mm sieve, still allows explaining high percentages of MTD variance. Furthermore, results demonstrate that the lower specification limits set up in technical specifications cannot be considered as good descriptors of the expected MTD. Indeed, they are greatly affected by a number of factors, including the variability of MTD for open-graded mixtures. Another point that emerges from the analyses is that for low-NMAS mixtures the impact of FV appears less important, while the impact of NMAS seems to be still important.

Further research is here needed because these types of mixtures are more and more used and tools are needed to better predict their MTD at the design stage. Results can benefit both researchers and practitioners.

Funding

The authors would like to thank all who sustained them with this research, especially the European Commission for its financial contribution to the LIFE20 ENV/IT/000181 (Project "SNEAK", optimized Surfaces against NoisE And vibrations produced by tramway tracK and road traffic) into the LIFE2020 programme, and the Italian Calabria Region (PAC Calabria 2014–2020).

References

[1] M. Merenda, F.G. Praticò, R. Fedele, R. Carotenuto, F.G. Della Corte, A real-time decision platform for the management of structures and infrastructures, Electron. 8 (2019). https://doi.org/10.3390/electronics8101180.

[2] F.G. Praticò, R. Vaiana, Improving infrastructure sustainability in suburban and urban areas: Is porous asphalt the right answer? And how?, in: WIT Trans. Built Environ., 2012. https://doi.org/10.2495/UT120571.

[3] F.G. Pratico, A. Moro, R. Ammendola, Modeling HMA bulk specific gravities: A theoretical and experimental investigation, Int. J. Pavement Res. Technol. 2 (2009) 115–122. https://doi.org/10.6135/ijprt.org.tw/2009.2(3).115.

[4] J.A. Ejsmont, G. Ronowski, B. Świeczko-Żurek, S. Sommer, Road texture influence on tyre rolling resistance, Road Mater. Pavement Des. 18 (2017). https://doi.org/10.1080/14680629.2016.1160835.

[5] S.V.A.R. Sastry, S.V.Y. Sastry, Comparison of the Overall Efficiency of the Cars at Different Speeds, Int. J. Emerg. Technol. Adv. Eng. 3 (2013) 509–512.

[6] S.S. Arkatkar, V.T. Arasan, Effect of gradient and its length on performance of vehicles under heterogeneous traffic conditions, J. Transp. Eng. 136 (2010). https://doi.org/10.1061/(ASCE)TE.1943-5436.0000177.

[7] F.G. Praticò, R. Vaiana, T. Iuele, Macrotexture modeling and experimental validation for pavement surface treatments, Constr. Build. Mater. 95 (2015) 658–666. https://doi.org/10.1016/j.conbuildmat.2015.07.061.

[8] ASTM E1845-15, Standard Practice for Calculating Pavement Macrotexture Mean Profile Depth, ASTM International, West Conshohocken, PA, 2015, Astm E1845. (2015) 1–4. https://doi.org/10.1520/E1845-15.2.

[9] B. M Gallaway, D.L. Ivey, G. Hayes, W.B. Ledbetter, R.M. Olson, Pavement and geometric design criteria for minimizing hydroplaning. Final Report (Phase 2)., (1979).

[10] V. Cerezo, M. Gothié, M. Menissier, T. Gibrat, Hydroplaning speed and infrastructure characteristics, Proc. Inst. Mech. Eng. Part J J. Eng. Tribol. 224 (2010). https://doi.org/10.1243/13506501JET738.

[11] H.S. Lee, D. Ayyala, Enhanced Hydroplaning Prediction Tool - FINAL REPORT, 2020.

[12] J. Chesterton, N. Nancekivell, N. Tunnicliffe, The Use of the Gallaway Formula for Aquaplaning Evaluation in New Zealand, in: NZIHT Transit NZ 8th Annu. Conf. 2006, 2006.

[13] M.R. Ahadi, K. Nasirahmadi, The Effect of Asphalt Concrete Micro & Macro Texture on Skid Resistance, 2013.

[14] R. Lamperti, Development of new methodologies for prediction of performances of asphalt mixtures, Alma Mater Studiorum – Università di Bologna, 2016.

[15] M.L. Afonso, M. Dinis-Almeida, C.S. Fael, Characterization of the Skid Resistance and Mean Texture Depth in a Permeable Asphalt Pavement, in: IOP Conf. Ser. Mater. Sci. Eng., 2019. https://doi.org/10.1088/1757-899X/471/2/022029.

[16] T. Wang, L. Hu, X. Pan, S. Xu, D. Yun, Effect of the compactness on the texture and friction of asphalt concrete intended for wearing course of the road pavement, Coatings. (2020). https://doi.org/10.3390/coatings10020192.

[17] B. Chen, C. Xiong, W. Li, J. He, X. Zhang, Assessing Surface Texture Features of Asphalt Pavement Based on Three-Dimensional Laser Scanning Technology, Buildings. 11 (2021) 21. https://doi.org/https://doi.org/10.3390/ buildings11120623.

[18] C. Plati, B. Cliatt, Building sustainable pavements: Investigating the effectiveness of recycled tire rubber as a modifier in asphalt mixtures, Energies. (2021). https://doi.org/10.3390/en14217099.

[19] N.R. Fisco, Comparison of Macrotexture Measurement Methods, The Ohio State University, 2009.

[20] S. Chen, X. Liu, H. Luo, J. Yu, F. Chen, Y. Zhang, T. Ma, X. Huang, A state-of-the-art review of asphalt pavement surface texture and its measurement techniques, J. Road Eng. 2 (2022) 156–180. https://doi.org/https://doi.org/10.1016/j.jreng.2022.05.003.

[21] J.C. Wambold, C.E.A. Statistician, J.J.H. Chairman, Z. Rado, PIARC - International piarc experiment to compare and harmonize texture and skid resistance measurements, 1995.

[22] ASTM, ASTM E1960-07: Standard Practice for Calculating International Friction Index of a

Pavement Surface, (2015). https://www.astm.org/e1960-07r15.html.

[23] C. Chen, F. Gu, M. Heitzman, B. Powell, K. Kowalski, Influences of alternative friction aggregates on texture and friction characteristics of high friction surface treatment, Constr. Build. Mater. 314 (2022). https://doi.org/10.1016/j.conbuildmat.2021.125643.

[24] L. Fuentes, M. Gunaratne, Revised methodology for computing international friction index, Transp. Res. Rec. (2011). https://doi.org/10.3141/2227-14.

[25] J.G. Rose, B.M. Gallaway, Water depth influence on pavement friction, ASCE Transp Eng J. 103 (1977). https://doi.org/10.1061/tpejan.0000648.

[26] T.F. Fwa, Determination and prediction of pavement skid resistance–connecting research and practice, J. Road Eng. 1 (2021). https://doi.org/10.1016/j.jreng.2021.12.001.

[27] K. Attenborough, Acoustical characteristics of rigid fibrous absorbents and granular materials, J. Acoust. Soc. Am. 73 (1983). https://doi.org/10.1121/1.389045.

[28] F.G. Praticò, Roads and Loudness: A More Comprehensive Approach, Road Mater. Pavement Des. 2 (2001) 359–377. https://doi.org/10.1080/14680629.2001.9689908.

[29] F.G. Praticò, R. Fedele, D. Vizzari, Significance and reliability of absorption spectra of quiet pavements, Constr. Build. Mater. 140 (2017) 274–281. https://doi.org/10.1016/j.conbuildmat.2017.02.130.

[30] J. Kragh, L.M. Iversen, U. Sandberg, NORDTEX FINAL REPORT Road Surface Texture for Low Noise and Low Rolling Resistance, 2013.

[31] CIRS, MINISTERO DEI LAVORI PUBBLICI (Italy) - CIRS - Centro Interuniversitario sperimentale di Ricerca Stradale - CAPITOLATO SPECIALE D'APPALTO TIPO PER LAVORI STRADALI - Art. 4, 5, and 6, (n.d.).

[32] ANAS, Capitolato Speciale di Appalto - Norme Tecniche per l'esecuzione del contratto - Parte 2, 2016.

[33] M. D'Apuzzo, A. Evangelisti, V. Nicolosi, Preliminary Findings for a Prediction Model of Road Surface Macrotexture, Procedia - Soc. Behav. Sci. 53 (2012).

https://doi.org/10.1016/j.sbspro.2012.09.960.

[34] L. Gao, M. Liu, Z. Wang, J. Xie, S. Jia, Correction of texture depth of porous asphalt pavement based on CT scanning technique, Constr. Build. Mater. (2019). https://doi.org/10.1016/j.conbuildmat.2018.12.154.

[35] J. Cesbron, S. Bianchetti, M.-A. Pallas, F.G. Praticò, R. Fedele, G. Pellicano, F. Bianco, A. Moro, Acoustical characterization of low-noise prototype asphalt concretes for electric vehicles, in: Euronoise 2021 (25-27 Oct. 2021, Madeira, Port. Online Conf., 2021: p. 10.

[36] ISO, Acoustics -- Specification of test tracks for measuring noise emitted by road vehicles and their tyres, Iso 10844. 2011 (2014) 54.

[37] Ecopneus, University of Pisa, Strati di usura con polverino da Pneumatici Fuori Uso per pavimentazioni stradali della viabilità urbana, 2019. https://www.ecopneus.it/wp-content/uploads/2019/04/17.-Ecopneus-Strati-di-usura-con-polverino-da-Pneumatici-Fuori-Uso-per-pavimentazioni-stradali-della-viabilità-urbana-specifiche-capitolati-appalto.pdf.

[38] F.G. Praticò, R. Fedele, P.G. Briante, Investigation on acoustic versus functional characteristics of porous asphalt, Balt. J. Road Bridg. Eng. 16 (2021). https://doi.org/10.7250/bjrbe.2021-16.546.

[39] J.N. Meegoda, G.M. Rowe, C.H. Hettiarachchi, N. Bandara, M.J. Sharrock, Correlation of Surface Texture, Segregation, and Measurement of Air Voids (NJDOT Research Project), 2002.

[40] D.A. Noyce, H.U. Bahia, J.M. Yambó, G. Kim, Incorporating Road Safety into Pavement Management: Maximizing Asphalt Pavement Surface Friction for Road Safety Improvements, Midwest Regional University Transportation Center (UMTRI), 2007.

[41] M. Skaf, E. Pasquini, V. Revilla-Cuesta, V. Ortega-López, Performance and durability of porous asphalt mixtures manufactured exclusively with electric steel slags, Materials (Basel). 12 (2019). https://doi.org/10.3390/ma12203306.

[42] R. Mistry, Circle Packing, Sphere Packing, and Kepler's Conjecture, 2016.

http://math.stmarys-ca.edu/wp-content/uploads/2017/07/Roshni-Mistry.pdf.

[43] European Standards, EN 13036-1 - Road and airfield surface characteristics - Test methods - Part 1: Measurement of pavement surface macrotexture depth using a volumetric patch technique, 2010.

[44] AASHTO, AASHTO T-312 - Standard Method of Test for Preparing and Determining the Density of Asphalt Mixture Specimens by Means of the Superpave Gyratory Compactor, 2019.

[45] European Standards, EN 12697-31 - Bituminous mixtures - Test methods - Part 31: Specimen preparation by gyratory compactor., 2019.

[46] ASTM, D6926-20 - Standard Practice for Preparation of Asphalt Mixture Specimens Using Marshall Apparatus, 2020. https://www.astm.org/d6926-20.html.

[47] European Standards, EN 12697-30 - Bituminous mixtures - Test methods - Part 30: Specimen preparation by impact compactor, 2018. https://standards.iteh.ai/catalog/standards/cen/9728dcfe-4137-454b-8765-63a37932df62/en-12697-30-2018.

[48] American Society for Testing Materials, Standard Test Method for Measuring Pavement Macrotexture Depth Using a, (2006) 1–4. https://doi.org/10.1520/E0965-96R06.2.

[49] F.G. Praticò, R. Vaiana, A study on the relationship between mean texture depth and mean profile depth of asphalt pavements, Constr. Build. Mater. 101 (2015) 72–79. https://doi.org/10.1016/j.conbuildmat.2015.10.021.

[50] AASHTO, Bulk Specific Gravity and Density of Compacted Hot Mix Asphalt (HMA) Using Automatic Vacuum Sealing Method, Aashto T 331. (2010).

[51] ASTM, D6752-09 - Standard Test Method for Bulk Specific Gravity and Density of Compacted Bituminous Mixtures Using Automatic Vacuum Sealing Method, 2011. https://www.astm.org/standards/d6752.